Response to reviewers

Reviewer 1

In this reply we comment on all remarks given by the reviewer and present the associated changes to the manuscript. The comments from each review have been copied into this document in grey and are marked with C for comment and a sequential number. The corresponding response is marked with R.

C1 There are two parts in this paper. The first part objective is to investigate the difference in basal shear stress from two models, one solving the Stokes equations (Elmer/Ice) and the second based on the 2nd order shallow ice approximation (iSOSIA), assuming the same glacier geometry. In the second part, using the iSOSIA model only, three different friction laws are compared on transient simulations accounting for bedrock erosion. The first part is used as a "validation" of the lower order model for the second part.

My main concern is on the way the two models are compared using vertically averaged velocity and stress, which looks not correct. For erosion, because processes take place at the interface between the ice and the bed, the quantities should not be vertically averaged, but instead one should take care to use the local values estimated at the bed/ice interface. I therefore not understand the necessity of averaging the velocity and stress from Elmer/Ice for the comparison with iSOSIA. Moreover, I suspect that by doing so, the differences between both models are decreased. The reverse should be done instead: the iSOSIA bedrock velocity and stress should be evaluated (this is always possible from a vertically integrated model to estimate the 3D velocity field, and then the 3D stress field), and the comparison conducted using velocity and stress at the bed.

R1 We thank the reviewer for the constructive comments. Based on the comments, we have modified the text and figures, and we feel this has improved the manuscript significantly.

The first comment is, however, based on a misunderstanding. Basal shear stress and basal sliding velocity are not, as understood by the reviewer, computed from depth-averaged properties. In both iSOSIA and Elmer/Ice, we extract the full Cauchy stress tensor at the bed, and use this to compute the bed-normal and -shear stress components from Eqn. 11.

Only the creep velocity shown in Fig. 1d and the horizontal longitudinal and transverse stress components in Fig. 2a are obtained by depth-averaging in both models. In Fig. 1d we can show the surface velocity instead, which would obviate depth-averaging of the creep-velocity. However, for the horizontal stress components, we can only compare depth-averaged values, as their depth-variation cannot be reconstructed from the iSOSIA output. We note, however, that focus is on the basal properties (bed shear stress and sliding rate, which are not based on depth-averaging anything in Elmer/Ice), and the horizontal stress plays a more indirect role in this study.

We realize that the text in section 2.4 (Comparing the output of iSOSIA and Elmer/Ice) has caused the misunderstanding. We have therefore rephrased text in this section to make it clearer that depth-averaging is not used for computing subglacial stress and sliding.

C2 all along the manuscript, Elmer/ICE should write Elmer/Ice (see e.g. Gagliardini et al., 2013).

R2 Elemer/ICE has been changed to Elmer/Ice throughout the manuscript.

C3 title: the title is a bit restrictive to the first part of the paper. You might think to a more general one that would include both objectives of the paper.

R3 The title was initially more general: "Glacial dynamics in response to glacial erosion". However, after advise from the associate editor, we changed this to specifically highlight the comparison study between iSOSIA and Elmer/Ice. We prefer the present title because it so clearly signals the study's focus on 1) basal shear stress and 2) computational models.

C4 p. 1144, l. 13: suble should be subtle?

R4 Done

C5 p. 1145, l. 16: These shear stress values should really be seen as mean value over a relatively large distance (>10m) as we know that, induced by cavitation for example, stress might concentrate at much higher values (e.g. Gagliardini et al., 2007), and that this stress concentration might play a key role in glacial erosion.

R5 This is true. We have rephrased the sentence to reflect this.

C6 p. 1148, 2.2: it should be mentioned if iSOSIA is a finite-element or finite-difference model.

R6 The iSOSIA implementation used here is a staggered-grid finite-difference model as explained in the second paragraph of section 2.2.

C7 p. 1148, l. 18: Stoke should write Stokes

R7 Done

C8 p. 1150, l. 2: the elevation used to compute the local temperature should not be bedrock elevation but the ice elevation when the bed is ice covered.

R8 We use bedrock elevation in the mass-balance equation in order to avoid that

a difference in sliding velocity, and hence ice thickness, influences the mass-balance. A constant and identical mass-balance function results in more transparent experiments, where secondary effects related to mass-balance do not mask the variations in stress caused by different sliding and erosion laws. We explain this in the paragraph below Eqn (3), and we have now strengthened this paragraph to more clearly motivate our choice of mass-balance function.

C9 p. 1151, Eqs. (6) and (7): what does justify the choice of an exponent 2 for the Weertman and Empirical sliding laws? In absence of cavitation, the exponent in the Weertman sliding law should be the Glen's exponent, so 3. I would suggest to adopt a different notation for Cs as the values are different for all three laws.

R9 A stress exponent of 2, or (n+1)/2, is in agreement with the model proposed by Weertman in 1957. For the empirical sliding law, exponents of both 2 and 3 seem to be commonly used. However, we agree with the reviewer that it makes sense to change the exponent from 2 to 3, also to increase the difference between the Weertman law and the empirical law (See also R22 below). The model experiment using the empirical sliding law (in experiment 3) has therefore been repeated (for erosion exponents of 1 and 2), and Figs. 8 and 9 have been updated.

C10 p. 1152, l. 14: extruded is may be more adapted than expanded. Also the number of vertical layers should be specified.

R10 This is a good suggestion. We now use extruded instead of expanded. The sentence already specifies the five vertical layers.

C11 p. 1152, Eq. (10): doing the comparison on vertically averaged values is not correct (see main point).

R11 See response to main point (R1)

C12 p. 1153, Eqs. (11) and (12): "×" should be replaced by "·".

R12 Yes, we agree. Done

C13 p. 1154, l. 20: I would suggest to plot relative difference instead of absolute one.

R13 We did try this, but we found the result to be misleading, mainly because areas of very low stress along the glacier margins result in very high relative errors (i.e. large difference of a very small number).
A plot of absolute difference allows the reader to assess the actual error. The reader can then estimate the level of the relative error without the bias of small numbers by comparing the levels of the stress difference to the levels of

actual stress.

C14 p. 1155, l. 18: remarkable should be remarkably

R14 Thank you. Done

C15 p. 1157, 3.3: Some explanation should be given on the way the sliding law parameters have been chosen. Did you try to get similar velocities for the initial geometry? Similar final geometries?

R15 Yes, we calibrated the constants to give a similar mean sliding velocity. This is now explained in section 3.3

C16 p. 1158, l. 4: m = 1 is in contradiction with what is specified in the Legend of Fig. 8 (m = 2). This should be corrected. If m = 2 in this experiment, then the sensitivity of the erosion exponent is not studied. You might think adding an experiment for all 3 friction laws with m = 1 (which must exist as you have results plotted in Fig. 9) .

R16 All experiments have been performed for both m=1 and m=2. We have modified the text to make this clear.

C17 p. 1158, l. 12: I would suggest to use equation instead of rule.

R17 Good idea. Done.

C18 p. 1161, l. 5-16: this is an important point which is discussed here, but I think it should not restricted to the Coulomb-friction law only. The parameter in all 3 friction laws would evolve if the bedrock topography evolve, but this is true that it is certainly at a sub-grid scale.

R18 This is another good point. We have expanded the discussion to include the other sliding laws as well.

C19 Figs. 7 and 8: For an easier comparison, the output should be produced for the same stages of glacial erosion (20, 60, 80, 100 for example).

R19 We agree. The figure has been updated.

C20 Table 1: "yr" should be "a"

R20 Done

C21 Fig. 9: does it make sense to use normalised mean velocity here as the erosion

is function of the absolute value of the velocity. At least, it should be mentioned how different are the mean velocity for the 3 friction laws at the beginning of the experiment.

R21 We have updated Fig. 9 to show absolute values. The trends are similar, but we agree that the absolute values add relevant information to the figure.

Response to reviewers

Reviewer 2

In this reply we comment on all remarks given by the reviewer and present the associated changes to the manuscript. The comments from each review have been copied into this document in grey and are marked with C for comment and a sequential number. The corresponding response is marked with R.
We thank the reviewer for positive and constructive comments. We have largely followed the reviewer's advice throughout.

C21 This is a useful and straightforward study that aims primarily to compare simulated fields of basal shear stress and sliding speed between two different models, for the purpose of informing landscape evolution models that employ glacial erosion. The 2-D depth-integrated high-order model iSOSIA (the 'home team' in this case) is compared to the 3-D Stokes model Elmer/Ice in two steady-state experiments, while sliding laws and erosion rules are compared in a third transient experiment that is restricted, for computational reasons, to iSOSIA.

The study is worthwhile, the results useful and the paper itself clear. The only scientific objection I have is in the design of the experiments themselves, or perhaps in the justification of the experimental design:

(1) I understand the rationale for using only iSOSIA in Experiment 3, but I don't under- stand why at least 2 sliding laws (Weertman/Budd-style and Coulomb friction) were not used with both models in Experiments 1 and 2. Using only the Weertman-style law for these experiments might limit the discrepancy between model results. Was the choice to exclude the Coulomb-friction law from Experiments 1 and 2 made for scientific or technical reasons?

R21 The comparison study between iSOSIA and Elmer/Ice was limited to the Weertman sliding law for technical reasons. In short, we were not able to make Elmer/Ice work in our setup with sliding laws that depend on effective pressure. We tried hard for a long period to make it work, but we were not able to make the solver converge, in spite of assistance from the Elmer team. We speculate that the challenge for Elmer/Ice arises when ice margins exist inside the FEM grid.
We did not want to discuss these technical issues too much in the manuscript, partly because we do not think that our problems with Elmer/Ice should keep others from trying. However, we understand that this info is important for motivating our experiments. We have therefore added sentences about this to section 2.3.
We will for the abovementioned reason not be able to supply additional Elmer/Ice experiments. However, we believe that 1) the comparison study based on Weertman sliding shows that the two solvers predict the same regional patterns of basal shear stress, and 2) the iSOSIA experiments using

three different sliding laws demonstrate that patterns of basal shear stress are robust and not overly sensitive to the choice of sliding law (Fig. 8).

C22 (2) I also wonder why two of three sliding laws tested were essentially the same, rather than choosing one in which sliding is linearly related to basal shear stress for example. Given the assumption of a uniform flotation fraction of 80% in order to compute N in (7), the Weertman law and the Budd law differ only by a factor that depends more or less on ice thickness (unless I have misunderstood something about the implementation here). One could argue that testing m=1 versus m=2 in the erosion law takes care of this, but only for the computed erosion rate rather than for the computed basal shear stress and sliding fields. Another means of differentiating the first two sliding laws would be to adopt a different flotation fraction to compute N. Does it make a difference?

R22 We agree that varying the stress exponent in the sliding laws more would increase the difference between experiments. We have thus increased the stress exponent in the empirical sliding law from 2 to 3 (See also response to comment C9 by reviewer 1) and repeated the experiments shown in Figs. 8 and 9). The details of the initial shear stress now vary a bit more, but the overall conclusions about regional patterns and the feedback from erosion remain the same.
We also agree that comparing models with different flotation fractions would complement the existing experiments nicely. We have therefore repeated the experiment using the Coulomb friction sliding law for two additional flotation fractions of 70% and 90%. We compare these to the model using 80% in a new figure (Fig. 10).

C23 (3) Finally, I wonder what difference it would make if the glacier geometry for Experiments 1 and 2 were created with Elmer/Ice rather than iSOSIA. Could the current methodology (creating topography with iSOSIA and then computing steady- state/diagnostic fields with both models for comparison) be responsible for some of the short-wavelength heterogeneity in the Elmer/Ice results (e.g. Fig. 2b and 2c)? The explanation given for the heterogeneity was that iSOSIA, due to its depth-averaging, would be expected to produce smoother results. It wasn't clear to me whether this was just a plausible explanation or one that had been demonstrated by the authors as the leading explanation.

I imagine that the authors may have done some of the tests suggested above already, and that there may be reasons not obvious to the reader (or this one at least) that the results were not mentioned or included. I think the paper would make a stronger case for the robustness of iSOSIA if it were put to what would seem more rigorous (though not more difficult or complicated) tests, as outlined above. At the very least, a better justification for the present experimental design would be appreciated.

R23 This is a good suggestion. We were not completely satisfied with our discussion of the high-frequency fluctuations in Elmer/Ice, because depth-averaging in iSOSIA should not make a big difference close to the bed. That Elmer/Ice was forced to use the iSOSIA ice configuration makes a better

explanation for the high-frequency variations, and we have now incorporated this in the text.

C24 1144.1: Suggest 'partially controls basal sliding' or 'exerts a significant control on basal sliding', since basal hydrology also plays a major (arguably dominant) role in some environments. Nice introduction.

R24 We agree. We now use "exerts a significant control on basal sliding".

C25 1149 (Section 2.3). The experimental set-up is generally described in this section and some differences between Expts 1-3 are mentioned (e.g. steady-state vs. transient). It would help to know exactly what the three experiments are in this section (e.g. purpose, which models), rather than having to wait until the beginning of each subsection of the results to find out.

R25 We have modified the text in the beginning of section 2.3 to motivate all three experiments upfront.

C26 1150.5: Figure 1b shows ice thickness, so might be better to say 'ice thickness distribution' than 'ice surface configuration'.

R26 Done

C27 1150.6-8: Given that the mass balance is specified as a function of bed topography (through the dependence of temperature on bed topography), it is unclear why there would be any mass-balance elevation feedback in the model unless the bed topography changes through time with isostasy.

R27 The feedbacks between bed topography and mass-balance are due to lowering of topography through erosion. We have now added this info to the relevant sentence.

C28 1151. Given that most of the paper focuses on modeled basal shear stress and sliding, it seems different exponents for (6) or (7) would be as or more important than different exponents for (9).

R28 We have changed the stress exponents of the empirical sliding model from 2 to 3 (see also R22 and R9)

C29 1154.3: Would be good to have this basic information on purpose and set-up of the Expt. before Results (i.e. in section 2.3).

R29 This is a good suggestion, and we have therefore moved much of this info to the beginning of section 2.3 (see also R25).

C30 1155.13-14 ‘reflects the influence of pressure. . .as well as vertical shear stress com- ponents’ I’m not sure what this explains. The basal shear stress dominates the force balance, as expected for a valley glacier, but. . . ?

R30 We can see the problem with this sentence. We have changed it to “The basal shear stress along the profile is 2 to 4 times greater in magnitude than the horizontal stress components, which highlights how basal shear stress dominates the force balance of valley glaciers”.

C31 1156.19: ‘rather uniform’. Here and elsewhere there is room for quantification of re- sults. Reporting the mean and standard deviation, for example, would be a better way of establishing this. See also paragraph below: ‘regional misfit remains small’.

R31 We have increased the level of quantification in this and other sentences. We now refer both to the mean and the standard deviation and several sentences that refer to Figs. 3 and 5.

C32 1157. Figure 6 could use an additional panel showing the difference between the two, or some field that would better convey the features mentioned in the text. Even annotating the existing figure would make it more instructive.

R32 We have added a third panel showing the total erosion. We have also annotated panel b) highlighting the trough, the hanging valleys, and truncated spurs.

C33 1158.8-10: The increased uniformity of basal shear stress only appears visibly obvious for the Weertman case. Perhaps some quantification of this effect would support the text that this effect is strongest for both Weertman and Coulomb-friction cases.

R33 It is true that the trend of decreasing shear stress with erosion is most obvious for the Weertman sliding law. However, the other two sliding laws follow the same trend. We now refer specifically to the quantified decrease in max shear stress for all sliding laws.

C34 Technical details (page.line):
1144.13: suble => subtle
1148.18: Stoke => Stokes
Eqn 1: divergence, not curl, of the flux
1149.17: ‘Ablation and accumulation are’
1152.2: ‘sliding-based erosion laws’
1155.2: correlate with => have
1155.18: remarkable => remarkably
1155.26: ‘driving stress . . . shows’
1156.7: Seems like both Figure 4b and 4c should be referenced here for ‘drainage patterns’, not just the sliding component (4b).
1156.14: ‘magnitude . . . increases’

1157.3: ‘in the order’ => ‘on the order’
1157.11: ‘costs . . . prevent’
1157.25: ‘development . . . causes’
1160.7-8: ‘bends ... that form’ ? [note sure to what ‘interlocking spurs’ refers]
1160.9-10: ‘erosion . . . removes’
1160.21: ‘features that resemble’
1160.22: reasonably => reasonable
1161.8: smoothened => smoothed
1162.3: suggest omitting ‘three-dimensional’. Not relevant to sentence, especially since some variables were depth-averaged for comparison with iSOSIA.
1162.11: ‘reduction in’ 1169.Table1: Coulomb mis-spelled 1174.Fig5 caption: Forth => Fourth

R34 We have followed the reviewers advice here and corrected all the above.

Manuscript prepared for Earth Surf. Dynam. Discuss.
with version 2014/09/16 7.15 Copernicus papers of the LaTeX class copernicus.cls.
Date: 10 January 2016

Basal shear stress under alpine glaciers: Insights from experiments using the iSOSIA and Elmer/~~ICE~~ Ice models

C. F. Brædstrup[1], D. L. Egholm[1], S. V. Ugelvig[1], and V. K. Pedersen[2]

[1]Department of Geoscience, Aarhus University, Høgh-Guldbergs gade 2, 8000 Aarhus, Denmark
[2]Department of Earth Sciences, University of Bergen, Allégaten 41, 5007 Bergen, Norway

Correspondence to: C. F. Brædstrup (christian@fredborg-braedstrup.dk) and D. L. Egholm (david@geo.au.dk)

Abstract

Shear stress at the base of glaciers ~~controls basal slidingand is therefore immensely important for glacial erosion and landscape evolution~~ exerts a significant control on basal sliding, and hence also glacial erosion in arctic and high-altitude areas. However, the inaccessible nature of glacial beds complicates empirical studies of basal shear stress, and little is therefore known of its spatial and temporal distribution.

In this study we seek to improve our understanding of basal shear stress using a higher-order numerical ice model (iSOSIA). In order to test the validity of the higher-order model, we first compare the detailed distribution of basal shear stress in iSOSIA and in a three-dimensional full-Stokes model (Elmer/~~ICE~~Ice). We find that iSOSIA and Elmer/~~ICE~~ Ice predict similar first-order stress and velocity patterns, and that differences are restricted to local variations ~~over~~ at length-scales on the order of the grid resolution. In addition, we find that subglacial shear stress is relatively uniform and insensitive to ~~suble~~ subtle changes in local topographic relief.

Following ~~these initial stress benchmark experiments~~the initial comparison studies, we use iSOSIA to investigate changes in basal shear stress as a result of landscape evolution by glacial erosion. The experiments with landscape evolution show that subglacial shear stress decreases as glacial erosion transforms preglacial V-shaped valleys into U-shaped troughs. These findings support the hypothesis that glacial erosion is most efficient in the early stages of glacial landscape development.

1 Introduction

The widespread late-Cenozoic glaciations produced distinctive glacial landforms in many mid- to high-latitude mountain ranges (e.g. Penck, 1905; Sugden and John, 1976). The glacial landforms include U-shaped valleys, bowl-shaped cirques, hanging valleys, and truncated spurs. The consistent geometry of these landforms and the associated non-fractal spatial scales show clear links to the dynamics of viscous flow (Evans and McClean, 1995;

Pelletier et al., 2010), which indicates that subglacial dynamics must be of first-order importance to ~~their~~ landscape evolution (e.g. Harbor et al., 1988; Anderson et al., 2006). However, measures of subglacial dynamics, such as basal shear and normal stress, are inherently difficult to obtain owing to the general inaccessibility of the subglacial environment.

A few studies have measured sliding velocity and basal stress directly; under Glacier d'Argentière in the French Alps (Boulton et al., 1979) and under Engabreen in Norway (Cohen et al., 2000, 2005; Iverson et al., 2003). These studies measured regional shear stress values between 0.1–0.3 MPa. However, interpretations from these studies are complicated by their limited spatial and temporal extent, and by local heterogeneity such as the presence of cavities that might concentrate stress at much higher values. It is therefore not possible to investigate catchment-wide variations in shear stress from these empirical studies. Knowledge of spatial and temporal variations in subglacial dynamics therefore rely mostly on inversion of geophysical data (e.g. Joughin et al., 2006, 2012; Habermann et al., 2013; Morlighem et al., 2013). Despite several complications in such studies (Joughin et al., 2004; Gudmundsson and Raymond, 2008; Habermann et al., 2012), and very different subglacial settings, these studies also find basal shear stress in the order of 0.1–0.4 MPa.

Numerical landscape evolution models are increasingly used to address fundamental questions relating to formation of glacial landscapes. The models can integrate erosional processes across the vast timescales of landscape evolution. This has improved the understanding of glacial valley evolution (Oerlemans, 1984; Harbor et al., 1988; Anderson et al., 2006; Herman et al., 2011), hanging-valley formation (MacGregor et al., 2000), as well as mountain-range height and relief development (Kessler et al., 2008; Egholm et al., 2009; Tomkin, 2009; Pedersen and Egholm, 2013; Pedersen et al., 2014). Moreover, recent studies have investigated the importance of glacial hydrology (Herman et al., 2011; Beaud et al., 2014), subglacial thermal regimes (Jamieson et al., 2008), sediment transport (Egholm et al., 2012), topographic control (Pedersen and Egholm, 2013; Pedersen et al., 2014), as well as feedbacks between different erosional processes (Braun et al., 1999; MacGregor et al., 2009; Egholm et al., 2015).

Although often hidden by results focussing on ~~sliding speed~~subglacial sliding rate, basal shear stress is an important underlying factor for scaling glacial erosion. Erosion rate is commonly assumed to scale with either basal sliding speed (e.g. Oerlemans, 1984; Harbor et al., 1988; Braun et al., 1999; Tomkin, 2009; Egholm et al., 2009; Herman et al., 2011) or ice discharge (e.g. MacGregor et al., 2000, 2009; Anderson et al., 2006; Kessler et al., 2008), and both depend on subglacial stress through sliding relations. Resolving variations in basal stress under glaciers is therefore important for modelling and understanding patterns of glacial erosion.

Ice motion can be computed using the Stokes equations ~~(?)~~ (Stokes, 1845) , which balance the stress components in the ice under the assumption of negligible inertia. Solving the full set of Stokes equations is a computationally demanding task, and most applications therefore use computationally efficient shallow-ice approximations (Mahaffy, 1976; Hutter, 1983; Blatter, 1995; Baral et al., 2001; Pattyn, 2003; Egholm et al., 2011). However, it is well known that the accuracy of these approximations depends strongly on the aspect ratio of the ice (ice thickness vs. horizontal extent), the bed slope, and horizontal gradients in ice velocity (Hutter, 1983; Baral et al., 2001).

As an end-member approximation, the zero'th-order shallow ice approximation (SIA) is computationally very efficient, but the approximation is only considered valid for the interior parts of large ice sheets where ice surface gradients are small and smoothly varying (Hutter, 1983; Le Meur et al., 2004; Hindmarsh, 2004). The limitation of SIA models arises mainly because the approximation ignores spatial stress gradients that provide regional coupling of ice flow across a glacier. The latter drawback has led to an increased use of higher-order shallow-ice models (HOM), which are considered more accurate in cases where ice velocity vary over relatively short distances (e.g. Pattyn, 2003; Hindmarsh, 2004; Egholm et al., 2011). However, the precise relationship between the aspect ratio of the ice and the accuracy of the shallow ice approximations is only vaguely defined. As a rule of thumb, the aspect ratio should be very small ($< 10^{-2}$) for a zero'th order approximation like SIA, while it may be higher (up to 1) for a second-order shallow ice approximation (Baral et al., 2001). Thus, although the higher-order ice dynamics of HOMs should increase accuracy compared

to SIA models in steep landscapes, they too will be challenged for example when bed slopes increase beyond a certain limit. These limitations and their implications have received little attention in alpine settings, despite being of prime importance to a number of areas in glaciology and landscape evolution.

Existing benchmark studies have compared results from different models (SIA to full-Stokes models) (Hubbard, 2000; Le Meur et al., 2004; Hindmarsh, 2004; Pattyn et al., 2008; Ahlkrona et al., 2013), but all have focused on simple descriptions of three-dimensional glacial landforms, often formulated by mathematical functions. ~~A~~Using data from the Haig Glacier in the Canadian Rocky Mountains, Adhikari et al. (2013) investigated the effects of higher-order dynamics for the future glacial evolution. Owing to the overdeepened bed, higher-order effects were suppressed as geometric constraints limited the horizontal glacial flow. In a recent study~~by Headley and Ehlers (2015)~~ , Headley and Ehlers (2015) compared two glacial models (a SIA model and a three-dimensional full-Stokes model) in a realistic landscape and found marked differences between models. As it is vital for predictions of ice flow and subglacial erosion to resolve subglacial stress accurately, we ~~perform new stress benchmark~~ performed new comparison experiments on a synthetic but realistic three-dimensional ~~fluvial~~ landscape using both the iSOSIA higher-order model and the Elmer/~~ICE~~ Ice full-Stokes model (Sect. 2.3). While this setup prevents analytical solution of the Stokes equations, it allows us to compare the iSOSIA approximation to a full-Stokes computational model in a realistic setting under different scales of relief (Sects. 3.1 and 3.2).

In subsequent experiments, the same ~~fluvial~~ landscape provides the basis for iSOSIA experiments that combine subglacial erosion with different models for basal sliding (Sect. 3.3). These final experiments are designed to explore long-term feedbacks between landscape evolution and subglacial dynamics.

2 Methods

In the following we introduce the ice models used in this study, along with technical details on experimental setup and model comparison.

2.1 Elmer/~~ICE~~Ice

The Elmer multi-physics software package (www.csc.fi/elmer) provides a finite-element framework for modelling both linear and non-linear three-dimensional flow problems. The Elmer software is developed at CSC in Finland with collaborators around the world, and is published under a GNU Public License (GPL). A special edition of Elmer, named Elmer/~~ICE~~Ice, is available with algorithms designed especially for problems related to ice flow (Gagliardini et al., 2013).

Elmer/~~ICE~~ Ice provides a highly accurate description of glacial dynamics by solving the full set of Stokes equations in three dimensions. However, the high degree of accuracy comes with a ~~very~~ high computational demand. Elmer is developed to run very efficiently in parallel (Gagliardini et al., 2013) to reduce computation time~~significantly~~, but the computations performed here still required ~~at least~~ two to three orders of magnitude more time than the corresponding SIA and iSOSIA simulations. Owing to the high computational demand, we only use Elmer/~~ICE~~ Ice to perform steady-state simulations without erosion.

2.2 iSOSIA

iSOSIA ~~has been~~ was developed specifically for modelling glacial landscape evolution (Egholm et al., 2011). The ice model includes all stress components of the ~~Stoke~~ Stokes equations. However, by using a second-order shallow ice approximation (Baral et al., 2001) iSOSIA represents a computationally efficient alternative to full-Stokes models. The main limiting assumption in iSOSIA is that horizontal, longitudinal and transverse stress components are not allowed to vary with depth in the ice. This assumption facilitates analytical depth-integration of velocities, and iSOSIA is hence a depth-integrated two-dimensional model.

The iSOSIA equations are highly non-linear because components of stress and ice velocity are connected through the non-Newtonian Glen's flow law for ice with a stress exponent of 3. The non-linear equations are relaxed using an iterative Red-Black finite-difference

Gauss–Seidel method (Briggs et al., 2000). iSOSIA was also recently ported to graphical processing units (GPU) with increased computational efficiency (Brædstrup et al., 2014).

2.3 Experimental Setup

All The first two experiments are designed to compare stress and velocity components from iSOSIA to those from Elmer/Ice. The objective is to test how well iSOSIA and Elmer/Ice agree on spatial variations in basal shear stress across gradients in topographic relief, ice thickness, and flow rate. The third experiment is used to study how patterns of basal shear stress and sliding evolve when topography change due to subglacial erosion. All three experiments are performed on a synthetic topography generated using a fluvial landscape evolution model based on stream-power erosion (Fig. 1a; Braun and Sambridge, 1997). This provides a particularly convenient setup where the uppermost drainage divide follows the grid boundaries, avoiding ice flow out of the model domain. The fluvial landscape has V-shaped valleys and concave longitudinal valley profiles that drain the landscape from a maximum elevation of 2500 m above sea-level down to 0 m (Fig. 1a). The computational grid is 20 by 40 km, consisting of 100 by 200 cells (i.e. 200 m resolution).

Ice thickness is time-integrated using the continuity equation,

$$\frac{\partial H}{\partial t} = -\nabla \times \cdot \boldsymbol{q} + M, \tag{1}$$

where H is ice thickness, t is time, $\boldsymbol{q}$ is ice flux, and M is the rate of ice accumulation/ablation.

Accumulation and ablation ~~is~~ are modelled as a simple linear function of atmospheric temperature:

$$M(x,y) = \begin{cases} -m_{\text{acc}}\, T(x,y), & \text{if } T(x,y) \leq 0, \\ -m_{\text{abl}}\, T(x,y), & \text{if } T(x,y) > 0, \end{cases} \tag{2}$$

where

$$T(x,y) = T_{\text{sl}} - \mathrm{d}T_h h(x,y) \tag{3}$$

is the atmospheric temperature. T_{sl} is the sea-level temperature, $\mathrm{d}T_h$ is the lapse rate, and h is bedrock elevation above sea level. m_{acc} is the accumulation gradient and m_{abl} is the ablation gradient. All values are listed in Table 1.

Experiments 1 and 2 assume steady state, and use the continuity equation only to construct the ~~ice surface~~ steady ice-thickness configuration (Fig. 1b). In experiment 3 the continuity equation is used to update ice thickness throughout transient simulations. However, in order to avoid that feedbacks between mass-balance, ice thickness, and topography influence the subglacial stress distribution, we use initial bed elevation in the mass-balance function, and we furthermore fix the mass balance in time and ignore the influence of topographical change by erosion on accumulation and ablation. This ~~allows us to more clearly study the direct influence of the evolving bed topography on subglacial stress under conditions of constant ice flux~~invariant mass-balance function prevents that secondary effects related to mass balance mask the differences in stress caused by different sliding and erosion laws.

Ice creep and basal sliding contribute to the ice flux vector, $\boldsymbol{q}$, in Eq. (1). The rate of ice creep is governed by Glen's flow law:

$$\dot{\varepsilon}_{ij} = A\tau_{\mathrm{e}}^{n-1} s_{ij}, \tag{4}$$

where $\dot{\varepsilon}_{ij}$ is the deviatoric strain rate tensor and s_{ij} is the deviatoric stress tensor. A and n are ice flow parameters (Table 1), and τ_{e} is the effective stress:

$$\tau_{\mathrm{e}} = \sqrt{s_{xz}^2 + s_{yz}^2 + s_{xy}^2 + \frac{1}{2}\left(s_{xx}^2 + s_{yy}^2 + s_{zz}^2\right)}, \tag{5}$$

iSOSIA uses a depth-integrated version of Glen's flow law to compute the depth-averaged flow velocities (Egholm et al., 2011).

The iSOSIA-Elmer/ice benchmarking experiments 1 and 2 use a simple Weertman sliding relation to relate basal shear stress to the rate of subglacial sliding. The Weertman relation was the only sliding model that successfully converged in Elmer/ice with our set-up. In experiment 3, however, we ~~make use of three different~~ combine iSOSIA with two additional sliding relations to examine the general sensitivity of subglacial stress to first-order assumptions on basal sliding velocity. The three sliding models are all represented by relations between basal shear stress and sliding velocity:

Weertman sliding: $\tau_{\mathrm{s}}^{\frac{1+n}{2}} = u_{\mathrm{s}}/C_{\mathrm{sw}}$ (Weertman, 1957) (6)

Empirical sliding: $\tau_{\mathrm{s}}^{2n} = u_{\mathrm{s}} N / C_{\mathrm{se}}$ (Budd et al., 1979) (7)

Columb-friction:Coulomb-friction: $\tau_{\mathrm{s}}/N = C_{\mathrm{sc}} \left(\dfrac{u_{\mathrm{s}}/N^n}{u_{\mathrm{s}}/N^n + \lambda_0} \right)^{1/n}$ (Schoof, 2005; Gagliardini et a (8)

Here τ_{s} is basal shear stress~~, C_{s} is a sliding coefficient~~; C_{w}, C_{e}, and C_{c} are sliding coefficients specific to each individual relation (Table 1), u_{s} is basal sliding velocity, and λ_0 is a constant defining the overall bed geometry in the Coulomb-friction sliding model

(Schoof, 2005; Gagliardini et al., 2007). The effective pressure, $N = t_n - p_w$, is the difference between the ice-bed normal stress, t_n, and water pressure, p_w. The two latter sliding relations (the empirical sliding model and ~~Columb-friction~~Coulomb-friction), which are both used in experiment 3, depend on effective pressure and hence subglacial water pressure. However, in order to focus on first-order correlations between topography and subglacial shear stress, we simplify the influence of hydrology and initially assume that water pressure is everywhere 80 % of the ice overburden pressure, $p_w = 0.8\rho_i g H$. In the final experiment we combine two additional flotation fractions of 70% and 90% with the Coulomb-friction sliding relation to test the influence of water pressure. We note, however, that more complex distributions of melt-water pressure may potentially affect patterns of subglacial shear stress through the influence of sliding (e.g. Flowers and Clarke, 2002; Werder et al., 2013; Beaud et al., 2014). Yet, such effects are beyond the scope of the present study.

In experiment 3 the glacier erodes its bed according to the following sliding-based erosion law:

$$\dot{e} = K_a |u_s|^m, \tag{9}$$

where $\dot{e}$ is erosion rate perpendicular to the bed, K_a is the erosion constant (Table 1), m is the erosion exponent and ~~u_s is sliding velocity~~u_s is sliding rate. Parameters governing subglacial erosion through abrasion and sliding are still being debated, and it is particularly relevant to question how well the sliding-based law represents subglacial quarrying (Iverson, 2012). However, sliding-based ~~erosions~~ erosion laws have been shown by models to produce realistic glacial landforms (Harbor, 1992; Seddik et al., 2005; Pedersen et al., 2014), which is why we use ~~it~~ one here to study how transformation of a landscape from fluvial-style to glacial-style influences the patterns of subglacial shear stress. Our use of the above erosion law is thus motivated more by phenomenological arguments ~~than emperical~~ (i.e. the erosion law leads to realistic glacial landforms) than empirical evidence. We ~~perform all erosional~~ do however perform all erosion experiments with both a linear ($m = 1$) and non-linear ($m = 2$) model in order to evaluate the robustness of our conclusions.

2.4 Comparing the output of iSOSIA and Elmer/~~ICE~~Ice

To ensure comparability between results produced by iSOSIA and Elmer/~~ICE~~Ice, both models operate on the same synthetic input topography, represented by a rectangular grid with specified bed elevation in each grid cell. The iSOSIA solver operates directly on this two-dimensional grid, whereas for Elmer/~~ICE~~ Ice the two-dimensional grid is ~~expanded~~ extruded to a full three-dimensional mesh with five vertical levels spanning the thickness of the ice. This gridding approach ensures that both models use exactly the same topographic input and mesh topology, except for Elmer/~~ICE~~ Ice having the additional vertical layering. In order to compare ice dynamics on exactly the same ice configuration, a steady-state ice distribution is generated using iSOSIA and subsequently used by both models. A free slip boundary condition is implemented along grid edges, and isothermal conditions are assumed everywhere in the grid.

~~Since Elmer/ICE computes stressand velocity on a three-dimensional grid, post-processing is necessary in order to compare with iSOSIA. Horizontal stress and flow componentsfrom Elmer/ICE are therefore~~ Both models compute basal shear stress,

$\boldsymbol{\tau}_\mathrm{s}$, from the Cauchy stress tensor, σ_b, at the bed:

$$\boldsymbol{\tau}_\mathrm{s} = \sigma_\mathrm{b} \cdot \boldsymbol{n}_\mathrm{b} - \boldsymbol{\sigma}_n, \tag{10}$$

where $\boldsymbol{\sigma}_n$ is the stress vector perpendicular to the bed:

$$\boldsymbol{\sigma}_n = (\boldsymbol{n}_\mathrm{b} \cdot \sigma_\mathrm{b} \cdot \boldsymbol{n}_\mathrm{b})\boldsymbol{n}_\mathrm{b}, \tag{11}$$

and $\boldsymbol{n}_\mathrm{b}$ is the normal vector at the bed:

$$\boldsymbol{n}_\mathrm{b} = \frac{1}{\ell_\mathrm{b}}\left[\frac{\partial b}{\partial x}, \frac{\partial b}{\partial y}, -1\right], \tag{12}$$

with

$$\ell_\mathrm{b} = \sqrt{1 + \left(\frac{\partial b}{\partial x}\right)^2 + \left(\frac{\partial b}{\partial y}\right)^2}. \tag{13}$$

We also compare the longitudinal and transverse stress components, s_{xx}, s_{yy}, and s_{xy} from both models. However, since these are only computed by iSOSIA in a depth-averaged version, we need to depth-average the horizontal stress also from Elmer/Ice. We obtain the depth-averaging using the following function:

$$\overline{s}_{xx} = \frac{1}{H}\int_0^H u s_{xx}(z)\mathrm{d}z, \tag{14}$$

~~where u is the variable of interest (stress or velocity component),~~ and similarly for $\overline{s}_{yy}$ and $\overline{s}_{xy}$. z is depth below the ice surface and H is local ice thickness.

~~Both models compute basal shear stress as:~~

$$\boldsymbol{\tau}_{\mathsf{s}} = \sigma_{\mathsf{b}} \times \boldsymbol{n}_{\mathsf{b}} - \boldsymbol{\sigma}_n,$$

~~where σ_{b} is~~ We note that for Elmer/Ice the depth-averaged stress components do not enter the Cauchy stress tensor ~~at the bed, and $\boldsymbol{\sigma}_n$ is the stress vector perpendicular to the bed:~~

$$\boldsymbol{\sigma}_n = (\boldsymbol{n}_{\mathsf{b}} \times \sigma_{\mathsf{b}} \times \boldsymbol{n}_{\mathsf{b}})\boldsymbol{n}_{\mathsf{b}},$$

~~$\boldsymbol{n}_{\mathsf{b}}$ is the normal vector at the bed:~~

$$\boldsymbol{n}_{\mathsf{b}} = \frac{1}{\ell_{\mathsf{b}}}\left[\frac{\partial b}{\partial x}, \frac{\partial b}{\partial y}, -1\right],$$

~~with~~

$$\ell_{\mathsf{b}} = \sqrt{1 + \left(\frac{\partial b}{\partial x}\right)^2 + \left(\frac{\partial b}{\partial y}\right)^2}.$$

in Eq. 15, which is instead constructed from the local stress state at the base of the ice.

In order to provide a frame of reference, we also compare the basal shear stress of iSOSIA and Elmer/~~ICE~~ Ice to the driving-stress approximation, which is used as a proxy for basal shear stress in zero'th order shallow ice approximations (Cuffey and Paterson, 2010). The driving stress is computed as,

$$\tau_{\mathsf{SIA}} = \rho_{\mathsf{i}} g H \sqrt{\left(\frac{\partial h}{\partial x}\right)^2 + \left(\frac{\partial h}{\partial y}\right)^2}, \tag{15}$$

where ρ_{i} is ice density, g is gravitational acceleration, H is ice thickness and h is the elevation of the ice surface.

3 Results

3.1 Experiment 1 – ~~benchmarking~~ comparing steady-state solutions

The first two experiments are used to benchmark stress and velocity components from iSOSIA against those from Elmer/~~ICE~~Ice. The steady-state ice configuration, which is first computed by iSOSIA and then used as input for both models, includes a main trunk glacier fed by several smaller tributary glaciers (Fig. 1b). Ice thickness reaches a maximum of 700 m in the main valley, and thins towards the glacier front and upwards in the tributaries. The depth-averaged creep velocity is highest where the ice is thickest in the main valley, reaching levels of 120 m a^{-1} (Fig. 1d). Basal sliding speed is high in the main valley and in the steeper parts of the high tributaries (Fig. 1c).

In experiment 1, the spatial distribution of stress is characterised by similar large-scale patterns in iSOSIA and Elmer/~~ICE~~ Ice (Fig. 2a). The components of horizontal normal stress, $\overline{s}_{xx}$ and $\overline{s}_{yy}$, are generally positive at high elevations, which reflects an overall extensional stress state in the accumulation zones. In the trunk valley at lower elevations, both stress components are in places negative (compressive) due to local deceleration of the ice. The latter tendency is however clearly affected by the details of the bed topography. The horizontal shear stress, $\overline{s}_{xy}$, is large, although of opposite sign, along both sides of the main valley due to a strong velocity gradient perpendicular to the main flow direction.

Differences between horizontal differential stress ($\overline{s}_{xx}$, $\overline{s}_{yy}$, and $\overline{s}_{xy}$) in Elmer/~~ICE~~ Ice and iSOSIA are in general below $\pm$0.03 MPa in tributary valleys and $\pm$0.01 MPa in the main valley (Fig. 2a, right column).

The basal shear stress is up to 0.2 MPa under the ice in the main trunk valley and near the tributary headwalls. Between these areas, basal shear stress is rather uniform at levels around 0.1 MPa. Differences between Elmer/~~ICE~~ Ice and iSOSIA are of order 0.025 MPa but up to 0.05 MPa in few areas (mostly along ice margins).

Sliding velocities are also similar in both models: $\sim$ 40 m yr^{-1} in the trunk valley and around 20 m yr^{-1} in the tributaries. Yet, the Elmer/~~ICE solution contains~~ Ice solution has areas with high-frequency variations in basal sliding and shear stress, which are absent

in the iSOSIA result. These areas ~~correlate with~~ have larger differences in sliding velocity between the two models (Fig. 2c, right column).

To aid the comparison between iSOSIA and Elmer/~~ICE~~ Ice we extract stress and velocity components along two profiles in the transverse and longitudinal directions of the valley (Fig. 3). The profile A-B runs directly across the main valley, while the profile C-D starts at high elevation and follows the ice drainage along the main valley down to sea-level.

The three horizontal stress components ($\overline{s}_{xx}$, $\overline{s}_{yy}$ and $\overline{s}_{xy}$) are all of order ± 0.04 MPa along the profiles, but vary in ways that reflect the bed topography. In the transverse direction (profile A-B, left panels of Fig. 3), stress components generally change sign in response to how the velocity components u_x and u_y vary across the valley (Fig. 1). The basal shear stress ~~, along the same profile ,~~ along the profile is 2 to 4 times greater in magnitude than the horizontal stress components, which ~~reflects the influence of pressure, p, as well as the vertical shear stress components s_{xz} and s_{yz}~~ highlights how basal shear stress dominates the force balance of valley glaciers.

Along the longitudinal profile (c and d, right panels in Fig. 3), the stress components also fluctuate around zero. A clear anti-correlation exists between $\overline{s}_{xx}$ and $\overline{s}_{yy}$, which indicate horizontal pure shear deformation in response to inflow of ice from the tributaries (Fig. 2a). The basal shear stress is ~~remarkable~~ remarkably constant along the profile and decreases only slightly up-glacier. This may seem surprising as bed slope increases significantly up-glacier. However, in this case, the effect of bed slope ~~seems in this case to be~~ is counteracted by ice thinning.

There are no clear trends in misfit between iSOSIA and Elmer/~~ICE~~ Ice and the two models generally predict the same patterns and magnitude of stress. Again, the main difference between results is that high-frequency stress variations are slightly larger for Elmer/~~ICE~~ Ice than for iSOSIA, particularly so for the basal shear stress (Figs. 2b and 3). As expected, the SIA driving stress is generally higher, and ~~show~~ shows more intense variation, than the basal shear stress for both iSOSIA and Elmer/~~ICE~~Ice.

3.2 Experiment 2 – the effect of relief

In the second experiment we gradually increase the total relief of the fluvial landscape to test how this influences the consistency between iSOSIA and Elmer/~~ICE~~ Ice results. Theoretically, increasing the relief should decrease the accuracy of iSOSIA as bed gradients and spatial variations in flow velocity intensify.

We use a simple scaling of the fluvial topography from experiment 1 in order to systematically increase the relief without affecting the drainage patterns (Fig. 4~~c~~). We then run iSOSIA to a steady-state ice configuration for all amplified topographies and transfer the resulting ice ~~thicknesses~~ thickness to Elmer/Ice in order to compute stress and velocity components under similar conditions.

When up-scaling relief, the ice-creep velocity increases significantly, the glacier thins, and its front margin advances (Fig. 4a). Because the ice-flow velocity is amplified almost uniformly, the magnitude of the horizontal stress components, which reflect local velocity gradients, also ~~increase~~ increases in response to the larger relief (Fig. 5). All three stress components still vary around 0 MPa, but the amplitude of the variation increases with relief. The largest response in horizontal stress due to increased relief, occurs in the steep high-elevation areas near the headwalls.

In contrast to the englacial horizontal stress, ~~the~~ basal shear stress is ~~remarkably~~ almost unaffected by the increasing relief and ~~remains rather uniform around 0.1–0.2~~the mean value remains around 0.2 MPa for all four situations (Fig. 5). The local deviation from this trend increases a bit from 0.02 to 0.05 MPa as the landscape steepens.

Examining differences between Elmer/~~ICE~~ Ice and iSOSIA, we note that both models agree on regional stress patterns, and that iSOSIA stress follows the Elmer/~~ICE~~ Ice solution reasonably well across the range of ~~reliefs~~ relief tested here. The regional misfit remains small (<0.02 MPa) even when maximum relief is 6250 m (Fig. 5c). There are however areas where the comparison exposes an increasing misfit (up to 0.1 MPa) between iSOSIA and Elmer/~~ICE~~Ice, particularly when focussing on variations at length scales of a few hundred

meters. These areas are mainly associated with thin ice and steep ice-surface topography near the glacial terminus or the headwall areas.

Unlike the basal shear stress from iSOSIA and Elmer/~~ICE~~Ice, both regional and local variations of SIA driving stress increase significantly with relief (Fig. 5, blue line). While the misfit between Elmer/~~ICE~~ Ice and iSOSIA are ~~in~~ on the order of 0–0.05 MPa for a relief of 5000 m (with spikes up to 0.1 MPa), the misfit between SIA and Elmer/~~ICE~~ Ice quickly reaches levels well above 0.2 MPa. This misfit is caused by the driving stress' lack of sensitivity to regional velocity variations as well as bed topography.

3.3 Experiment 3 – evolution of stress under glacial erosion

After evaluating steady-state solutions of iSOSIA against Elmer/~~ICE~~ Ice we now investigate the long-term transient evolution of basal shear stress in response to subglacial erosion and landscape development. We only ~~use~~ used iSOSIA for this experiment as the computational costs of Elmer/~~ICE prevents~~ Ice prevent us from running simulations over the thousand year ~~timescales~~ time-scales required for glacial landscape development. The initial topography from experiment 1 ~~is~~ was used as input for iSOSIA and ~~is~~ was slowly eroded using a sliding-based erosion law (Eq. 9).

First, we ~~run~~ ran the experiment using the Weertman relation for sliding (Eq. 6; Weertman, 1957) in combination with a non-linear erosion law ($m = 2$ in Eq. 9). We find that the V-shaped fluvial valley structure is transformed into a wider and steep-sided U-shaped trough (Fig. 6). This is in agreement with previous studies (Harbor, 1992; Seddik et al., 2005; Egholm et al., 2012). Several other characteristic glacial landforms also appear as a result of glacial erosion, including steep and narrow upper ridges, flattened valley floors, hanging valleys and truncated spurs (Fig. 6b).

As expected, bed slopes increase in many areas of the landscape, particularly along valley sides and near headwalls (Fig. 7). However, along the longitudinal flowline of the glacier, bed slopes generally decrease as glacial erosion flattens the valley floor and removes bedrock features that obstruct flow. This development generally ~~cause~~ causes bed shear stress to decrease in amplitude and become more uniformly distributed under the ice

(Fig. 7). ~~This~~ The reduction in basal shear stress also decreases sliding velocity as a result of the Weertman sliding relation (Eq. 6; Fig. 7).

To test the robustness of this trend we ~~repeat~~ repeated experiment 3 using two additional sliding relations: the empirical relation (Eq. 7; Budd et al., 1979) and the Coulomb-friction relation (Eq. 8; Schoof, 2005; Gagliardini et al., 2007)~~as well as a linear erosion law ($m = 1$ in Eq. 9)~~. The different sliding coefficients (Table 1) were calibrated to give similar average rates of sliding.

The three sliding relations predict slightly different distributions of subglacial shear stress, but all agree on the first-order patterns and magnitudes (Fig. 8). All three relations ~~initially lead to high values of~~ predict high shear stress in the trunk valley and upper tributaries, and short-scale stress variations that mimic the details of the valley morphology. With increased erosion all sliding relations lead to decreased and more uniformly distributed basal shear stress. This effect is strongest for the Weertman ~~and Columb-friction~~ relation but occur for all three relations. As a consequence of the decreasing stress, the spatially averaged sliding velocity also exhibits an overall decrease with erosion in the trunk valley ~~, which~~ (Fig. 9a).

To further test the robustness of this trend, we repeated the experiments using: 1) a linear erosion law ($m = 1$ in Eq. 9) in combination with all three sliding laws (Fig. 9b), and 2) the Coulomb-friction sliding model using two alternative flotation fractions (70% and 90%) to compute effective pressure, N (Fig. 9c).

The similar outcome of these final experiments suggests that decreasing basal shear stress in response to erosion is largely independent of hydrology and the exponent, m, in the erosion ~~rule~~ equation (Fig. 9). The latter ~~underlines~~ indicates that first-order topographical change is more important than the details of the erosion law.

4 Discussion

4.1 The benchmarking experiments

In order to estimate the practical utility of iterative higher-order shallow-ice approximations, we have compared the results of two different computational methods: iSOSIA and Elmer/~~ICE~~Ice. The comparison experiments were designed to reflect a realistic setting of relevance for long-term glacial landscape-evolution studies. However, the realism of the experiments, involving complex topographical variations, also means that we cannot obtain any exact solution for the stress or velocity distributions, and therefore cannot quantify the true accuracy of any of the two computational methods. Instead, the objective of the ~~benchmarking experiments~~ comparison study is to estimate the ~~difference~~ difference between stress predicted by the two methods under conditions that are as similar as possible, and we have designed the experiments to meet this criteria. Both methods use the same bed topography and ice distribution, as well as the same horizontal Cartesian grid structure (with an additional vertical grid-dimension for Elmer/~~ICE~~Ice). We note here that the true accuracy of both methods is expected to depend on grid resolution. For example, the finite-element method in Elmer/~~ICE~~ Ice allows irregular grid structures that may increase the computational accuracy, e.g. along ice margins where steep ice surface gradients call for increased spatial resolution (Durand et al., 2011). However, a comparison study designed to uncover the difference caused by various approximations to the Stokes equations is ~~not~~ only meaningful if similar meshes are ~~not~~ used.

The ~~benchmark experiments show~~ comparison study shows that iSOSIA and Elmer/~~ICE~~ Ice predict the same overall patterns of stress and velocity. In both models, components of horizontal stress and stress gradients interact with flow patterns on a regional scale (i.e. across topographical gradients, which is in strong contrast to the driving stress in SIA models). This highlights, in accordance with previous studies (e.g. Le Meur et al., 2004; Hindmarsh, 2004; Egholm et al., 2011, 2012), the benefits of HOM and full-Stokes models over SIA models. The main difference in results from iSOSIA and Elmer/~~ICE~~ Ice seems to be confined to spatial scales of few hundred meters (i.e. the ~~grid cell~~ grid-cell spacing).

In particular, Elmer/~~ICE~~ Ice includes high-frequency fluctuations in basal shear stress and sliding (Fig. 2) whereas the iSOSIA results appear more smoothly varying. The smoother pattern in iSOSIA is perhaps not surprising when considering the inherent depth-integration of horizontal stress. On the other hand, the relatively large differences in sliding velocity between neighbouring grid cells in Elmer/~~ICE~~ Ice are surprising and cannot ~~easily~~ readily be explained by variations in bed topography.

We therefore ascribe these high-frequency stress variations in Elmer/Ice to the ice thickness configuration used, which was generated using iSOSIA and therefore in balance with the governing equations of this ice model. Elmer/Ice is not allowed to make adjustments to the ice thickness, that would otherwise dampen the local stress variations.

The high-frequency variations of Elmer/~~ICE~~ Ice are amplified slightly when the total catchment relief increase from 2500 to 7500 m (Fig. 5). On the other hand, the more regional accordance between iSOSIA and Elmer/~~ICE~~ Ice stress predictions seems almost unaffected by the increasing relief. This is in contrast to the SIA driving stress, which rises with increasing relief.

4.2 The evolution of stress in response to erosion

The iSOSIA simulations with erosion (experiment 3) suggest that variations in basal shear stress are generally reduced by the gradual transformation from a fluvial to a glacial topography. ~~We observe this trend~~ This trend can be recognized for all sliding laws tested in this study (Weertmann, empirical, ~~Columb-friction~~Coulomb-friction; Fig. 8) and for two different sliding exponents in the erosion law.

The highest ~~initial levels of~~ basal shear stress ~~are~~ is associated with bends in the fluvial channel profile that ~~forms~~ form interlocking spurs (Fig. 7). These spurs are truncated by glacial erosion ~~which~~ and this decreases basal shear stress. In the main valley, glacial erosion thereby efficiently ~~remove~~ removes obstacles and straightens the path of ice flow. In addition to this, glacial erosion flattens the longitudinal valley profile and widens its cross section, which also contributes to reduced basal shear stress (Harbor, 1992; Seddik et al., 2005).

It is not surprising in the current study, that the modelled glacial erosion primarily attacks portions of the glacial bed where basal shear stress is high. Basal shear stress is connected to sliding rate through ~~the sliding relations~~ a sliding relation (Eqs. 6–8), which, in turn, is assumed to scale rates of erosion (Eq. 9). We note that different rules for glacial erosion, for example the ones based on mechanics of bedrock quarrying (Iverson, 2012), could depend differently on sliding and shear stress. Feedbacks between stress and erosion might be different in such cases. On the other hand, the experiments presented here result in topographic features that ~~resembles~~ resemble well-known glacial landforms, and it seems ~~reasonably~~ reasonable that smoother and flatter post-glacial landforms are associated with less drag from the ice.

With increased erosion, the resulting decrease in basal shear stress leads in our experiment to a lowering of sliding rate, and hence slowdown of erosion. This is a direct consequence of the sliding relations used. ~~Two~~ All of the sliding relations have a power-law scaling between stress and sliding, and sliding must decrease with decreasing shear stress (the ~~Weertman and the empirical sliding relations). The~~ power-law scaling of the Coulomb-friction sliding model ~~, on the other hand, operates with~~ occurs below an upper limit to the bed's ability to support shear stress~~(the bed resistance~~). In addition to the sliding rate, ~~the upper stress limit (the bed resistance) associated with Coulomb-friction depends on water pressure and the bed~~ basal shear stress associated with the sliding models depends on bed resistance and roughness, which is controlled by parameters ~~C_s~~ C_w, C_e, C_c and λ_0 in ~~Eq~~Eqs. (6–8). Here we speculate, that if ~~the~~ bed resistance decreases more rapidly than the shear stress imposed on the bed by the ice flow, then sliding may possibly accelerate as ~~the~~ topography is eroded, in contrast to the results presented here. The bed resistance could decrease if, for example, the bed is ~~smoothened~~ smoothed by erosion or if the flatter glacial longitudinal valley profile reduces the melt-water drainage efficiency of the glacier. Our experiment 3 does not show such behaviour, partly because we ignore complex effects of melt-water hydrology, and partly because the sliding parameters representing bed roughness ~~(C_s and λ_0 in Eq. 8)~~ are treated as constants independent of erosion. However, understanding how glacial erosion affects the topographical conditions that promote cavita-

tion on length scales below the current grid resolution of landscape evolution models, may be important for advancing our understanding of feedbacks between glacial dynamics and topographical development.

Because of general lowering of basal shear stress with erosion, our results support the hypothesis that glacial erosion is most efficient in the initial phase of glacial landscape evolution, ~~when landforms are unadapted~~ before landforms are adapted to the new glacial regime (Harbor, 1992; Braun et al., 1999). In general, however, landscape evolution is influenced by several processes not accounted for here, such as a transient climate forcing (Pedersen and Egholm, 2013), changing topography due to a tectonic forcing (e.g. Tomkin and Braun, 2002), periglacial processes acting in concert with glacial erosion (e.g. Egholm et al., 2015), fluvial processes and mass wasting affecting the landscape especially during ice-free interglacial periods (e.g. Schlunegger and Hinderer, 2003), and subglacial fracturing in response to high differential ~~in situ~~ stresses (e.g. Leith et al., 2014).

5 Conclusions

We have investigated and compared the spatial distribution of subglacial shear stress in both a higher-order shallow-ice model (iSOSIA) and a full-Stokes ~~three-dimensional~~ model (Elmer/~~ICE~~Ice). Using iSOSIA only, we also investigated the temporal evolution of basal shear stress in response to subglacial erosion. In total, we conducted three experiments in order to resolve different aspects of subglacial shear stress. We found that,

- iSOSIA and Elmer/~~ICE~~ Ice produce stress and sliding patterns that are largely similar under the conditions tested.
- In the alpine setting used here, basal shear stress seems rather insensitive to increases in overall relief, as reduction ~~on~~ in ice thickness counteracts the effects of bed steepening. Thus, increasing total relief by a factor 3 only produces a small response in basal shear stress.

– Subglacial erosion removes obstacles that give rise to high basal shear stress in the pre-glacial landscape setting. By this, glacial erosion leads to lower and more uniformly distributed basal shear stress.

– Using three different sliding relations and two different erosion laws, we find a stabilising feedback between basal shear stress, sliding, erosion, and topography. This feedback depends however on constant sliding coefficients, which in a more realistic setting could be altered by long-term changes to the bed roughness.

Author contributions. C. F. Brædstrup and D. L. Egholm designed the study, developed the computational tools and conducted iSOSIA experiments. C. F. Brædstrup was responsible for work with Elmer/Ice. C. F. Brædstrup and D. L. Egholm prepared the manuscript with contributions from co-authors.

Acknowledgements. We thank Thomas Zwinger from the Elmer/~~ICE~~ Ice team for invaluable help with ~~initial model setup. This research~~ model set-up. Associate editor Michelle Koppes and two anonymous reviewers are thanked for constructive comments and suggestions that improved the manuscript. The study was funded by The Danish Council for Independent Research under the Sapere Aude program.

References

Adhikari, S., and Marshall, S. J.: Influence of high-order mechanics on simulation of glacier response to climate change: insights from Haig Glacier, Canadian Rocky Mountains, The Cryosphere, 7, 1527–1541, doi:10.5194/tc-7-1527-2013, 2013.

Ahlkrona, J., Kirchner, N., and Lötstedt, P.: Accuracy of the zeroth- and second-order shallow-ice approximation – numerical and theoretical results, Geosci. Model Dev., 6, 2135–2152, doi:10.5194/gmd-6-2135-2013, 2013.

Anderson, R. S., Molnar, P., and Kessler, M. A.: Features of glacial valley profiles simply explained, J. Geophys. Res.-Earth, 111, F01004, doi:10.1029/2005JF000344, 2006.

Baral, D. R., Hutter, K., and Greve, R.: Asymptotic theories of large-scale motion, temperature, and moisture distribution in land-based polythermal ice sheets: a critical review and new developments, Appl. Mech. Rev., 54, 215–256, 2001.

Beaud, F., Flowers, G. E., and Pimentel, S.: Seasonal-scale abrasion and quarrying patterns from a two-dimensional ice-flow model coupled to distributed and channelized subglacial drainage, Geomorphology, 219, 176–191, 2014.

Blatter, H.: Velocity and stress fields in grounded glaciers: a simple algorithm for including deviatoric stress gradients, J. Glaciol., 41, 333–344, 1995.

Boulton, G., Morris, E., Armstrong, A., and Thomas, A.: Direct measurement of stress at the base of a glacier, J. Glaciol., 22, 3–24, 1979.

Braun, J. and Sambridge, M.: Modelling landscape evolution on geological time scales: a new method based on irregular spatial discretization, Basin Res., 9, 27–52, doi:10.1046/j.1365-2117.1997.00030.x, 1997.

Braun, J., Zwartz, D., and Tomkin, J.: A new surface-processes model combining glacial and fluvial erosion, Ann. Glaciol., 28, 282–290, 1999.

Brædstrup, C. F., Damsgaard, A., and Egholm, D. L.: Ice-sheet modelling accelerated by graphics cards, Comput. Geosci., 72, 210–220, doi:10.1016/j.cageo.2014.07.019, 2014.

Briggs, W. L., Henson, V. E., and McCormick, S. F.: A Multigrid Tutorial, SIAM, Philadelphia, PA, USA, 2000.

Budd, W. F., Keage, P. L., and Blundy, N. A.: Empirical studies of ice sliding, J. Glaciol., 23, 157–170, 1979.

Cohen, D., Hooke, R. L., Iverson, N. R., and Kohler, J.: Sliding of ice past an obstacle at Engabreen, Norway, J. Glaciol., 46, 599–610, 2000.

Cohen, D., Iverson, N., Hooyer, T., Fischer, U., Jackson, M., and Moore, P.: Debris-bed friction of hard-bedded glaciers, J. Geophys. Res.-Earth, 110, F02007, doi:10.1029/2004JF000228, 2005.

Cuffey, K. M. and Paterson, W.: The Physics of Glaciers, 4th edn., Academic Press, Burlington, Massachusetts, USA, 2010.

Durand, G., Gagliardini, O., Favier, L., Zwinger, T., and le Meur, E.: Impact of bedrock description on modeling ice sheet dynamics, Geophys. Res. Lett., 38, L20501, doi:10.1029/2011GL048892, 2011.

Egholm, D. L., Nielsen, S. B., Pedersen, V. K., and Lesemann, J.-E.: Glacial effects limiting mountain height, Nature, 460, 884–887, 2009.

Egholm, D. L., Knudsen, M. F., Clark, C. D., and Lesemann, J. E.: Modeling the flow of glaciers in steep terrains: The integrated second-order shallow ice approximation (iSOSIA), J. Geophys. Res.-Earth, 116, F02012, doi:10.1029/2010JF001900, 2011.

Egholm, D., Pedersen, V., Knudsen, M., and Larsen, N.: On the importance of higher order ice dynamics for glacial landscape evolution, Geomorphology, 141–142, 67–80, 2012.

Egholm, D. L., Andersen, J. L., Knudsen, M. F., Jansen, J. D., and Nielsen, S. B.: The periglacial engine of mountain erosion – Part 2: Modelling large-scale landscape evolution, Earth Surf. Dynam. Discuss., 3, 327–369, doi:10.5194/esurfd-3-327-2015, 2015.

Evans, I. S. and McClean, C. J.: The land surface is not unifractal; variograms, cirque scale and allometry, Z. Geomorphol., 101, 127–147, 1995.

Flowers, G. E. and Clarke, G. K. C.: A multicomponent coupled model of glacial hydrology., 1. Theory and synthetic examples, J. Geophys. Res.-Sol. Ea., 107, ECV 9–1–17, doi:10.1029/2001JB001122, 2002.

Gagliardini, O., Cohen, D., Råback, P., and Zwinger, T.: Finite-element modeling of subglacial cavities and related friction law, J. Geophys. Res.-Earth, 112, F02027, doi:10.1029/2006JF000576, 2007.

Gagliardini, O., Zwinger, T., Gillet-Chaulet, F., Durand, G., Favier, L., de Fleurian, B., Greve, R., Malinen, M., Martín, C., Råback, P., Ruokolainen, J., Sacchettini, M., Schäfer, M., Seddik, H., and Thies, J.: Capabilities and performance of Elmer/Ice, a new-generation ice sheet model, Geosci. Model Dev., 6, 1299–1318, doi:10.5194/gmd-6-1299-2013, 2013.

Gudmundsson, G. H. and Raymond, M.: On the limit to resolution and information on basal properties obtainable from surface data on ice streams, The Cryosphere, 2, 167–178, doi:10.5194/tc-2-167-2008, 2008.

Habermann, M., Maxwell, D., and Truffer, M.: Reconstruction of basal properties in ice sheets using iterative inverse methods, J. Glaciol., 58, 795–807, 2012.

Habermann, M., Truffer, M., and Maxwell, D.: Changing basal conditions during the speed-up of Jakobshavn Isbræ, Greenland, The Cryosphere, 7, 1679–1692, doi:10.5194/tc-7-1679-2013, 2013.

Harbor, J. M.: Numerical modeling of the development of U-shaped valleys by glacial erosion, Geol. Soc. Am. Bull., 104, 1364–1375, 1992.

Harbor, J. M., Hallet, B., and Raymond, C. F.: A numerical model of landform development by glacial erosion, Nature, 333, 347–349, doi:10.1038/333347a0, 1988.

Headley, R. M. and Ehlers, T. A.: Ice flow models and glacial erosion over multiple glacial–interglacial cycles, Earth Surf. Dynam., 3, 153–170, doi:10.5194/esurf-3-153-2015, 2015.

Herman, F., Beaud, F., Champagnac, J.-D., Lemieux, J.-M., and Sternai, P.: Glacial hydrology and erosion patterns: A mechanism for carving glacial valleys, Earth Planet. Sc. Lett., 310, 498–508, 2011.

Hindmarsh, R. C. A.: A numerical comparison of approximations to the Stokes equations used in ice sheet and glacier modeling, J. Geophys. Res.-Earth, 109, F01012, doi:10.1029/2003JF000065, 2004.

Hubbard, A.: The verification and significance of three approaches to longitudinal stresses in high-resolution models of glacier flow, Geogr. Ann. A, 82, 471–487, 2000.

Hutter, K.: Theoretical Glaciology: Material Science of Ice and the Mechanics of Glaciers and Ice Sheets, Springer, New York, USA, 1983.

Iverson, N. R.: A theory of glacial quarrying for landscape evolution models, Geology, 40, 679–682, doi:10.1130/G33079.1, 2012.

Iverson, N. R., Cohen, D., Hooyer, T. S., Fischer, U. H., Jackson, M., Moore, P. L., Lappegard, G., and Kohler, J.: Effects of basal debris on glacier flow, Science, 301, 81–84, 2003.

Jamieson, S. S. R., Hulton, N. R. J., and Hagdorn, M.: Modelling landscape evolution under ice sheets, Geomorphology, 97, 91–108, 2008.

Joughin, I., MacAyeal, D. R., and Tulaczyk, S.: Basal shear stress of the Ross ice streams from control method inversions, J. Geophys. Res.-Sol. Ea., 109, B09405, doi:10.1029/2003JB002960, 2004.

Joughin, I., Bamber, J. L., Scambos, T., Tulaczyk, S., Fahnestock, M., and MacAyeal, D. R.: Integrating satellite observations with modelling: basal shear stress of the Filcher–Ronne ice streams, Antarctica, Philos. T. R. Soc. A., 364, 1795–1814, doi:10.1098/rsta.2006.1799, 2006.

Joughin, I., Smith, B. E., Howat, I. M., Floricioiu, D., Alley, R. B., Truffer, M., and Fahnestock, M.: Seasonal to decadal scale variations in the surface velocity of Jakobshavn Isbrae, Greenland: Observation and model-based analysis, J. Geophys. Res.-Earth, 117, , f02030, doi:10.1029/2011JF002110, 2012.

Kessler, M. A., Anderson, R. S., and Briner, J. P.: Fjord insertion into continental margins driven by topographic steering of ice, Nat. Geosci., 1, 365–369, 2008.

Le Meur, E., Gagliardini, O., Zwinger, T., and Ruokolainen, J.: Glacier flow modelling: a comparison of the Shallow Ice Approximation and the full-Stokes solution, C. R. Phys., 5, 709–722, 2004.

Leith, K., Moore, J. R., Amann, F., and Loew, S.: Subglacial extensional fracture development and implications for Alpine Valley evolution, J. Geophys. Res.-Earth, 119, 62–81, doi:10.1002/2012JF002691, 2014.

MacGregor, K. R., Anderson, R., Anderson, S., and Waddington, E.: Numerical simulations of glacial-valley longitudinal profile evolution, Geology, 28, 1031–1034, 2000.

MacGregor, K. R., Anderson, R. S., and Waddington, E. D.: Numerical modeling of glacial erosion and headwall processes in alpine valleys, Geomorphology, 103, 189–204, 2009.
Mahaffy, M. W.: A three-dimensional numerical model of ice sheets: tests on the Barnes Ice Cap, Northwest Territories, J. Geophys. Res., 81, 1059–1066, 1976.
Morlighem, M., Seroussi, H., Larour, E., and Rignot, E.: Inversion of basal friction in Antarctica using exact and incomplete adjoints of a higher-order model, J. Geophys. Res.-Earth, 118, 1746–1753, doi:10.1002/jgrf.20125, 2013.
Oerlemans, J.: Numerical experiments on large-scale glacial erosion, Z. Gletscherkunde und Glazialgeologie, 20, 107–126, 1984.
Pattyn, F.: A new three-dimensional higher-order thermomechanical ice sheet model: basic sensitivity, ice stream development, and ice flow across subglacial lakes, J. Geophys. Res.-Sol. Ea., 108, EPM 4–1, doi:10.1029/2002JB002329, 2003.
Pattyn, F., Perichon, L., Aschwanden, A., Breuer, B., de Smedt, B., Gagliardini, O., Gudmundsson, G. H., Hindmarsh, R. C. A., Hubbard, A., Johnson, J. V., Kleiner, T., Konovalov, Y., Martin, C., Payne, A. J., Pollard, D., Price, S., Rückamp, M., Saito, F., Souček, O., Sugiyama, S., and Zwinger, T.: Benchmark experiments for higher-order and full-Stokes ice sheet models (ISMIP–HOM), The Cryosphere, 2, 95–108, doi:10.5194/tc-2-95-2008, 2008.
Pedersen, V. K. and Egholm, D. L.: Glaciations in response to climate variations preconditioned by evolving topography, Nature, 493, 206–210, 2013.
Pedersen, V. K., Huismans, R. S., Herman, F., and Egholm, D. L.: Controls of initial topography on temporal and spatial patterns of glacial erosion, Geomorphology, 223, 96–116, 2014.
Pelletier, J. D., Comeau, D., and Kargel, J.: Controls of glacial valley spacing on Earth and Mars, Geomorphology, 116, 189–201, 2010.
Penck, A.: Glacial features in the surface of the Alps, J. Geol., 13, 1–19, 1905.
Schlunegger, F. and Hinderer, M.: Pleistocene/Holocene climate change, re-establishment of fluvial drainage network and increase in relief in the Swiss Alps, Terra Nova, 15, 88–95, 2003.
Schoof, C.: The effect of cavitation on glacier sliding, P. Roy. Soc. A-Math. Phy., 461, 609–627, doi:10.1098/rspa.2004.1350, 2005.
Seddik, H., Sugiyama, S., and Naruse, R.: Numerical simulation of glacial-valley cross-section evolution, B. Glaciol. Res., 22, 75–79, 2005.
Stokes, G. G.: On the theories of the internal friction of fluids in motion and of the equilibrium and motion of elastic solids, Trans. Cambridge Philos. Soc., 8, 287–319, 1845.
Sugden, D. E. and John, B. S.: Glaciers and Landscape, Edward Arnold, London, England, 1976.

Tomkin, J. H.: Numerically simulating alpine landscapes: the geomorphologic consequences of incorporating glacial erosion in surface process models, Geomorphology, 103, 180–188, 2009.
Tomkin, J. H. and Braun, J.: The influence of alpine glaciation on the relief of tectonically active mountain belts, Am. J. Sci., 302, 169–190, 2002.
Weertman, J.: On the sliding of glaciers, J. Glaciol., 3, 33–38, 1957.
Werder, M. A., Hewitt, I. J., Schoof, C. G., and Flowers, G. E.: Modeling channelized and distributed subglacial drainage in two dimensions, J. Geophys. Res.-Earth, 118, 2140–2158, 2013.

Table 1. Model parameters used for all experiments.

Parameters		Value unit
ρ_{i}	Ice Density	$910.0\,\mathrm{kg\,m^{-3}}$
$\mathrm{d}T_h$	Atmospheric lapse rate	$6.0\,^{\circ}\mathrm{C\,km^{-1}}$
g	Acceleration of gravity	$9.82\,\mathrm{m\,s^{-2}}$
A	Ice flow parameter	$1 \times 10^{-16}\,\mathrm{Pa^{-3}\,a^{-1}}$
n	Ice flow stress exponent	3
~~C_{s}~~ C_{w}	Weertman sliding coefficient	$2 \times 10^{-9}\,\mathrm{m\,Pa^{-2}\,a^{-1}}$
~~C_{s}~~ C_{e}	Empirical sliding coefficient	~~2×10^{-3}~~ $5 \times 10^{-9}\,\mathrm{m\,Pa^{-2}\,a^{-1}}$
~~C_{s}~~ C_{c}	~~Columb-friction~~ Coulomb-friction sliding coefficient	0.25
λ_0	~~Columb-friction~~ Coulomb-friction sliding parameter	$2 \times 10^{-17}\,\mathrm{m\,Pa^{-3}\,a^{-1}}$
m_{acc}	Accumulation gradient	$0.5\,\mathrm{m\,a^{-1}\,^{\circ}C^{-1}}$
m_{alb}	Ablation gradient	$1.5\,\mathrm{m\,a^{-1}\,^{\circ}C^{-1}}$
T_{sl}	Sea-level temperature	$6\,^{\circ}\mathrm{C}$
K_{a}	Subglacial abrasion erosion constant	
	for $m = 1$	8×10^{-5}
	for $m = 2$	$2.5 \times 10^{-6}\,\mathrm{m^{-1}\,a}$
m	Subglacial erosion exponent	1–2

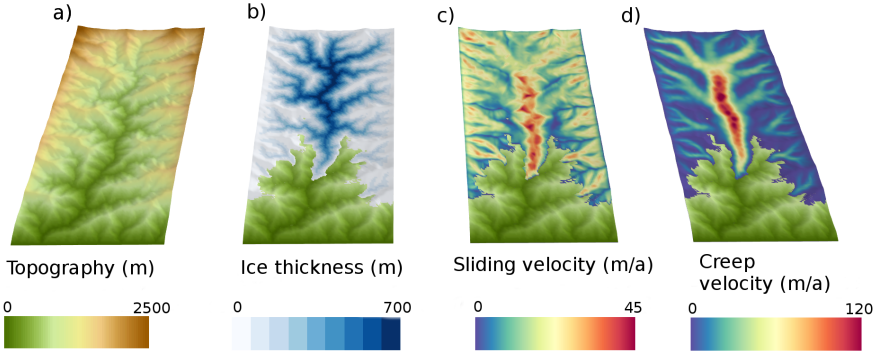

Figure 1. Bed topography **(a)**, steady-state ice thickness **(b)**, sliding velocity **(c)**, and depth-averaged creep velocity **(d)** for experiment 1. The velocities shown are from iSOSIA.

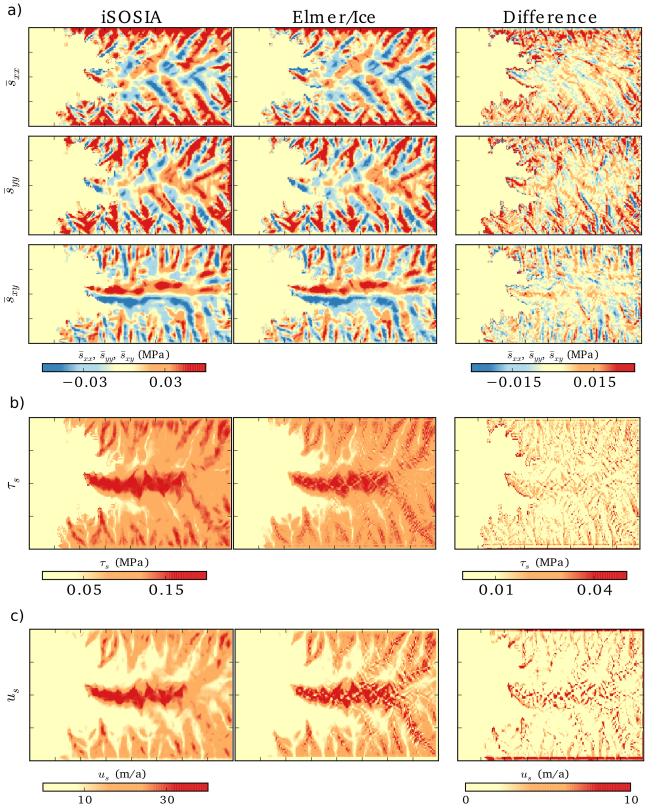

Figure 2. (a) Comparison of stress components from iSOSIA and Elmer/~~ICE~~ Ice shown in top view. The first two columns show the depth-averaged stress components $\overline{s}_{xx}$, $\overline{s}_{yy}$, and $\overline{s}_{xy}$. The right-most column shows the difference between iSOSIA and Elmer/~~ICE~~ Ice results. **(b)** Basal shear stress for both models. **(c)** Sliding velocity using a Weertman relation (Eq. 6). Ice flow is from right to left.

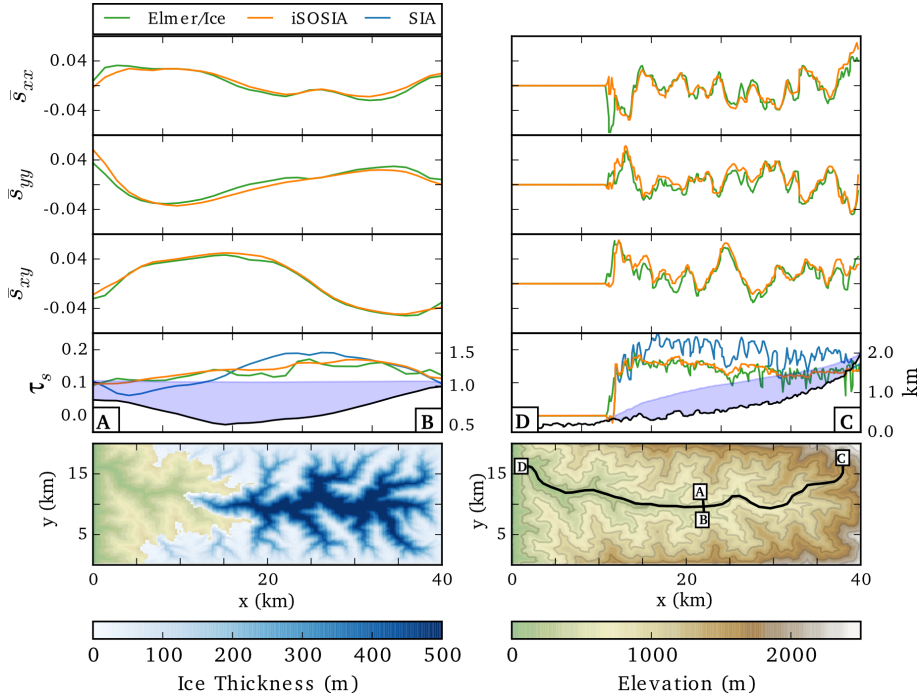

Figure 3. iSOSIA (orange) and Elmer/~~ICE~~ Ice (green) stress components in MPa along a transverse (left column) and a longitudinal (right column) profile~~in~~. Upper three rows compare the higher-order depth-averaged horizontal stress components. The fourth row shows the basal shear stress along the same profiles. The SIA driving stress (Eq. 15) is also shown for comparison (blue line). The fourth row also shows bed topography (black line) and ice thickness (blue shaded area). Notice that elevation is indicated on right axis. Bottom left panel shows ice thickness. The position of the two profiles (A–B and C–D) are shown in the bottom right panel. Note that the bottom row are map views of the 3D model (Fig. 1a, b).

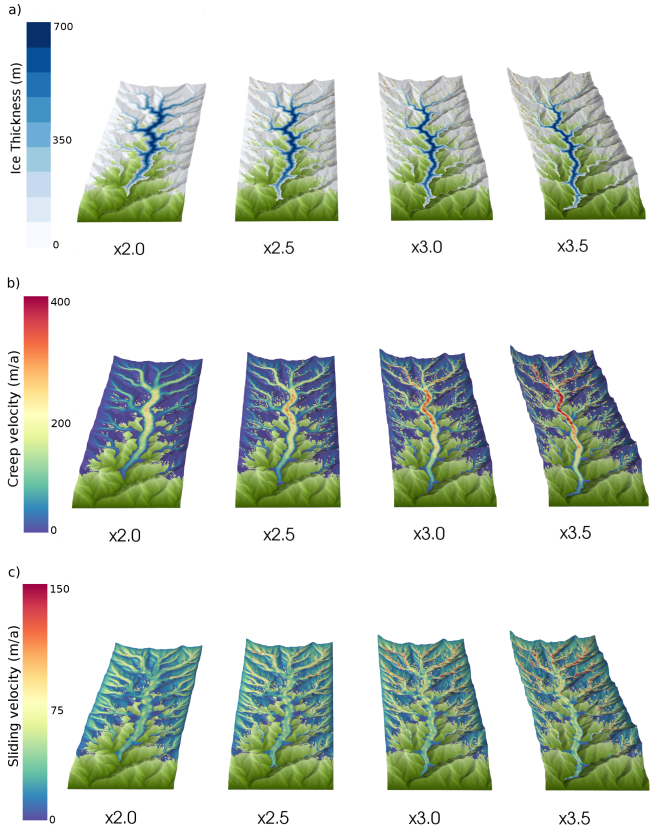

Figure 4. Bed topography with ice cover **(a)**, creep velocity **(b)**, and basal sliding velocity **(c)** computed at steady-state using iSOSIA for the four scaling factors in experiment 2. The total relief is 3750, 5000, 6250, and 7500 m respectively.

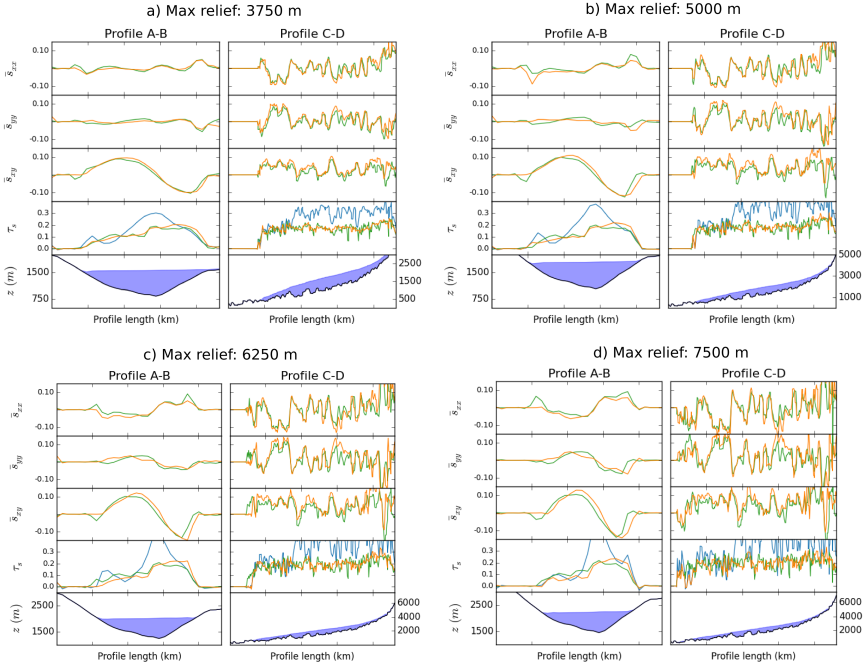

Figure 5. Stress components in MPa from iSOSIA (orange) and Elmer/~~ICE~~ Ice (green) for the increasing topographical relief in experiment 2. Left column of each panel **(a–d)** shows values along the transverse profile A–B, while the right column is along the longitudinal profile C–D (Fig. 3). The SIA driving stress approximation is also shown in the third row for comparison (blue line). ~~Forth~~ Fourth row shows the ice-surface and bed topography along the same profiles. Note that elevation is indicated on the left and right axis respectively.

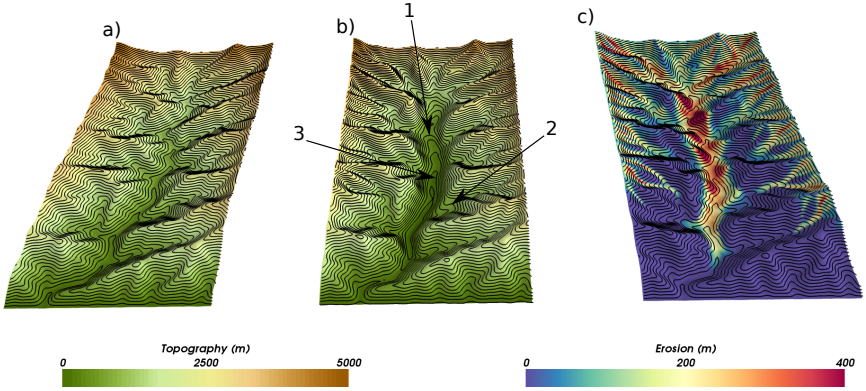

Figure 6. textbf(a) Preglacial landscape ~~showing the~~ with initial fluvial topography~~(a)~~. **(b)** The ~~postglacial~~ landscape after 100 m ~~of~~ average glacial erosion (using $m = 2$ in Eq. 9) . ~~**(b).**~~ Several characteristic ~~features of glaciated landscapes~~ glacial landforms are evident in ~~**(b)**~~the eroded landscape. Highlighted with numbered arrows are: (1) flattened valley floor, (2) a hanging valley, and (3) a truncated spur. The ~~trunk~~ main valley is widened forming a U-shaped cross-section with steep slopes along the sides~~forming a U-shaped cross section~~. ~~Flattened~~ **(c)** The total bedrock erosion. Erosion is concentrated in the main trunk valley ~~floors, hanging valleys and~~ along the truncated spurs ~~are also visible~~and at high elevation near the headwalls of tributary glaciers.

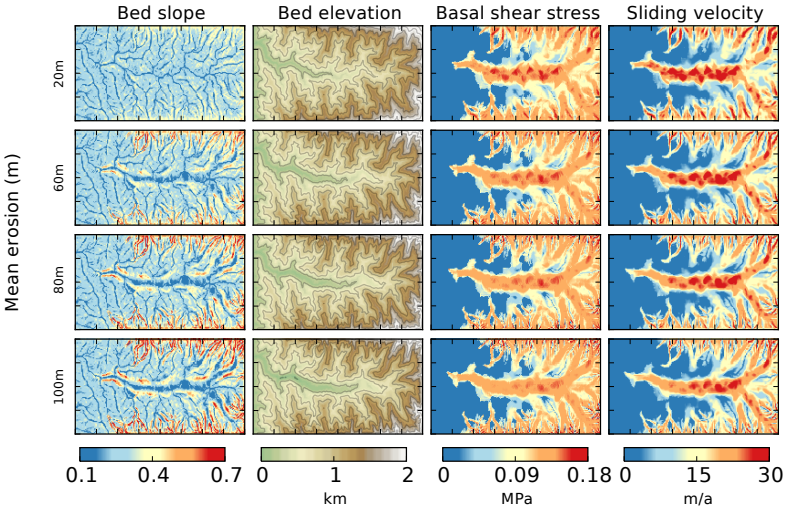

Figure 7. The results from experiment 3 with glacial erosion and using the Weertman sliding relation (Eq. 6) and $m = 2$ in Eq. (9). Each column shows bed slope, bed elevation, basal shear stress and basal sliding speed at different stages of erosion.

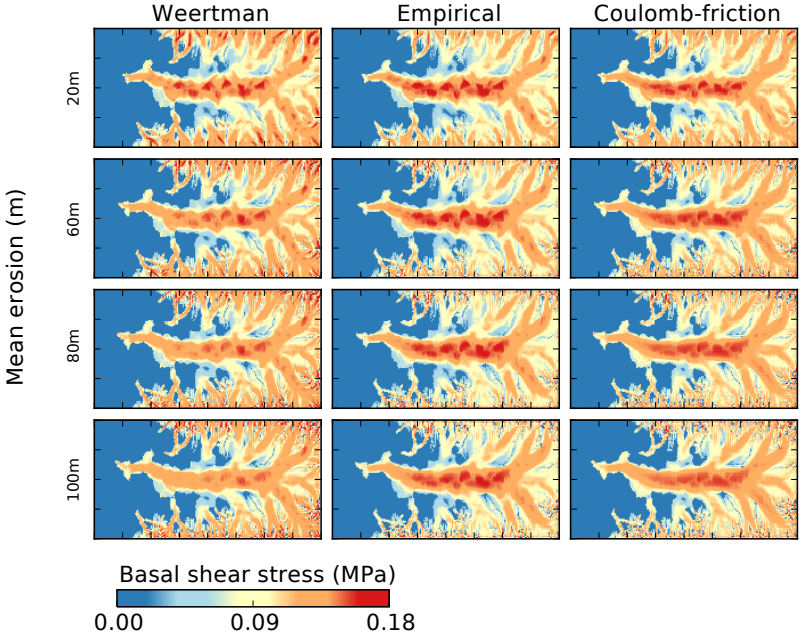

Figure 8. Results from experiment 3 using different sliding relations and $m = 2$ in Eq. (9). The three columns show basal shear stress for the different sliding laws: Weertman (Eq. 6), empirical (Eq. 7) and ~~Columb-friction~~ Coulomb-friction (Eq. 8) at different stages of glacial erosion.

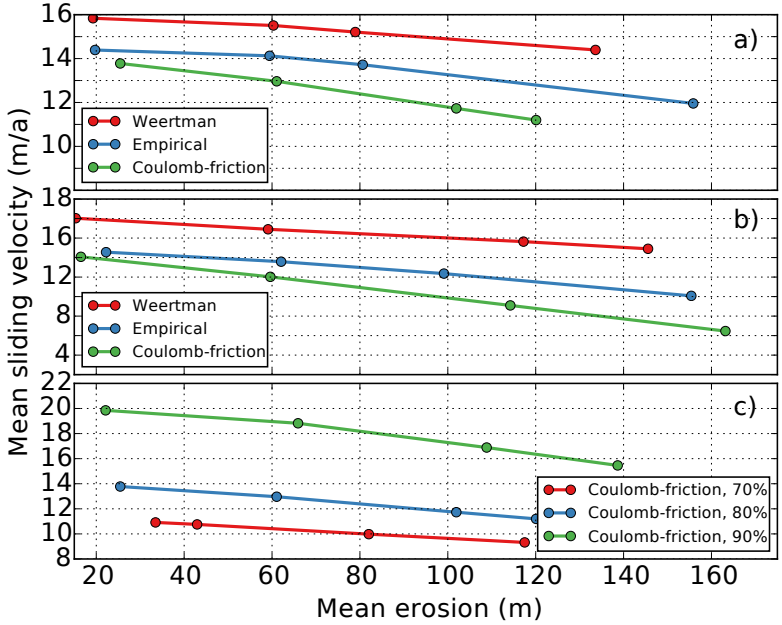

Figure 9. Evolution of ~~normalised~~ mean sliding rate as a function of mean erosion. **(a)** Shows results for three different sliding laws ~~. **(a)** Shows results~~ using a ~~linear~~ non-linear erosion law (~~$m = 1$~~ $m = 2$ in Eq. 9) and 80% floatation. **(b)** ~~Results using $m = 2$~~The same as **(a)** but for $m = 1$. **(c)** The evolution of mean sliding for the Coulomb-friction sliding law and three different levels of floatation. The means of sliding rate and erosion are computed only for the trunk valley, defined as all glaciated cells below 750 m elevation in the initial fluvial landscape.

```
a6c6
<   experiments using the iSOSIA and Elmer/ICE models}
---
>   experiments using the iSOSIA and Elmer/Ice models}
16c16
< \runningtitle{The evolution of glacial dynamics}
---
> \runningtitle{Basal shear stress under alpine glaciers}
20c20
< \correspondence{C.~F.~Br{\ae}dstrup (christian.fredborg@geo.au.dk)
---
> \correspondence{C.~F.~Br{\ae}dstrup (christian@fredborg-braedstrup.dk)
32,34c32,33
<   Shear stress at the base of glaciers controls basal sliding and is
<   therefore immensely important for glacial erosion and landscape
<   evolution in arctic and high-altitude areas. However, the
---
>   Shear stress at the base of glaciers exerts a significant control on
>   basal sliding, and hence also glacial erosion in arctic and high-altitude areas. Howe
43,44c42,43
<   a~three-dimensional full-Stokes model (Elmer/ICE). We find that
<   iSOSIA and Elmer/ICE predict similar first-order stress and velocity
---
>   a~three-dimensional full-Stokes model (Elmer/Ice). We find that
>   iSOSIA and Elmer/Ice predict similar first-order stress and velocity
46c45
<   over length-scales on the order of the grid resolution. In addition,
---
>   at length-scales on the order of the grid resolution. In addition,
48c47
<   insensitive to suble changes in local topographic relief.
---
>   insensitive to subtle changes in local topographic relief.
50c49
<   Following these initial stress benchmark experiments, we use iSOSIA
---
>   Following the initial comparison studies, we use iSOSIA
69c68
< dynamics must be of first-order importance to their evolution
---
> dynamics must be of first-order importance to landscape evolution
79c78
< \citep{cohen2000,cohen2005,iverson2003}. These studies measured shear
---
> \citep{cohen2000,cohen2005,iverson2003}. These studies measured regional shear
83c82
< cavities.  It is therefore not possible to investigate catchment-wide
---
> cavities that might concentrate stress at much higher values.  It is
therefore not possible to investigate catchment-wide
110c109
< Although often hidden by results focussing on sliding speed, basal
---
> Although often hidden by results focussing on subglacial sliding rate, basal
122d120
<
124c122
< \citep{stokes1845}, which balance the stress components in the ice
---
> \citep{Stokes1845}, which balance the stress components in the ice
164,165c162,168
< glacial landforms, often formulated by mathematical functions.
< A~recent study by \citet{headley2015} compared two glacial models
---
```

```
> glacial landforms, often formulated by mathematical functions. Using
> data from the Haig Glacier
> in the Canadian Rocky Mountains, \cite{adhikari2013} investigated the
> effects of higher-order dynamics for the future glacial evolution. Owing to the
> overdeepened bed, higher-order effects were suppressed as geometric
> constraints limited the horizontal glacial flow.
> In a~recent study, \cite{headley2015} compared two glacial models
167c170,171
< landscape and found marked differences between models.  As it is vital
---
> landscape and found marked differences between models.
> As it is vital
169,171c173,174
< subglacial stress accurately, we perform new stress benchmark
< experiments on a~synthetic but realistic three-dimensional fluvial
< landscape using both the iSOSIA higher-order model and the Elmer/ICE
---
> subglacial stress accurately, we performed new comparison
experiments on a~synthetic but realistic three-dimensional
> landscape using both the iSOSIA higher-order model and the Elmer/Ice
178c181
< In subsequent experiments, the same fluvial landscape provides the
---
> In subsequent experiments, the same landscape provides the
189c192
< \subsection{Elmer/ICE}
---
> \subsection{Elmer/Ice}
197c200
< Elmer, named Elmer/ICE, is available with algorithms designed
---
> Elmer, named Elmer/Ice, is available with algorithms designed
200c203
< Elmer/ICE provides a~highly accurate description of glacial dynamics
---
> Elmer/Ice provides a~highly accurate description of glacial dynamics
202,206c205,206
< dimensions. However, the high degree of accuracy comes with a~very
< high computational demand. Elmer is developed to run very efficiently
< in parallel \citep{elmer2013} to reduce computation time
< significantly, but the computations performed here still required at
< least two to three orders of magnitude more time than the
---
> dimensions. However, the high degree of accuracy comes with a~high
computational demand. Elmer is developed to run very efficiently
> in parallel \citep{elmer2013} to reduce computation time, but the
computations performed here still required two to three orders of
magnitude more time than the
208c208
< computational demand, we only use Elmer/ICE to perform steady-state
---
> computational demand, we only use Elmer/Ice to perform steady-state
214c214
< iSOSIA has been developed specifically for modelling glacial landscape
---
> iSOSIA was developed specifically for modelling glacial landscape
216c216
< stress components of the Stoke equations. However, by using
---
> stress components of the Stokes equations. However, by using
236c236,237
< All experiments are performed on a~synthetic topography generated
---
> The first two experiments are designed to compare stress and velocity
```

```
> components from iSOSIA to those from Elmer/Ice. The objective is to
test how well iSOSIA and Elmer/Ice agree on spatial variations in
basal shear stress across gradients in topographic relief, ice
thickness, and flow rate. The third experiment is used to study how
patterns of basal shear stress and sliding evolve when topography
change due to subglacial erosion.  All three experiments are performed
on a~synthetic topography generated
245,246c246,247
< of 100 by 200 cells (i.e. 200\,\unit{m} resolution).
<
---
> of 100 by 200 cells (i.e. 200\,\unit{m} resolution).\\
>
249c250
<  \frac{\partial H}{\partial t}=-\nabla\times\vec{q}+M,\label{eq:cont}
---
>  \frac{\partial H}{\partial t}=-\nabla\cdot\vec{q}+M,\label{eq:cont}
254c255
< Accumulation and ablation is modelled as a~simple linear function of
---
> Accumulation and ablation are modelled as a~simple linear function of
272c273
< gradient. All values are listed in Table~\ref{tab:settings}.
---
> gradient. All values are listed in Table~\ref{tab:settings}.
275c276
< equation only to construct the ice surface configuration
---
> equation only to construct the steady ice-thickness configuration
278,283c279,282
< However, in order to avoid that feedbacks between mass-balance and
< topography influence the subglacial stress distribution, we fix the
< mass balance in time and ignore the influence of topographical change
< on accumulation and ablation. This allows us to more clearly study the
< direct influence of the evolving bed topography on subglacial stress
< under conditions of constant ice flux.
---
> However, in order to avoid that feedbacks between mass-balance, ice thickness, and
> topography influence the subglacial stress distribution, we use
initial bed elevation in the mass-balance function, and we furthermore fix the
> mass balance in time and ignore the influence of topographical change by erosion
> on accumulation and ablation. This invariant mass-balance function
prevents that secondary effects related to mass balance mask the
differences in stress caused by different sliding and erosion laws.
301c300
< The benchmarking experiments 1 and 2 use a~simple Weertman sliding
---
> The iSOSIA-Elmer/ice benchmarking experiments 1 and 2 use a~simple Weertman sliding
303,304c302,303
< sliding. In experiment 3, however, we make use of three different
< sliding relations to examine the sensitivity of subglacial stress to
---
> sliding. The Weertman relation was the only sliding model that
successfully converged in Elmer/ice with our set-up. In experiment 3,
however, we combine iSOSIA with two additional
> sliding relations to examine the general sensitivity of subglacial stress to
309,311c308,310
< & \text{Weertman sliding:} \,\,\,   \tau_{\mathrm{s}}^2 =
u_{\mathrm{s}}/C_{\mathrm{s}} \label{eq:weertman} \quad  \text{(Weertman,~1957)} \\
< & \text{Empirical sliding:}\,\,\,   \tau_{\mathrm{s}}^2 =
< u_{\mathrm{s}} N/C_{\mathrm{s}} \label{eq:budd}   \quad  \text{(Budd
---
> & \text{Weertman sliding:} \,\,\,   \tau_{\mathrm{s}}^\frac{1+n}{2}
= u_{\mathrm{s}}/C_{\mathrm{w}} \label{eq:weertman} \quad  \text{(Weertman,~1957)} \\
```

```
> & \text{Empirical sliding:}\,\,\,   \tau_{\mathrm{s}}^n =
> u_{\mathrm{s}} N/C_{\mathrm{e}} \label{eq:budd}   \quad  \text{(Budd
313c312
< & \text{Columb-friction:} \,\,\,  \tau_{\mathrm{s}}/N  = C_{\mathrm{s}}
---
> & \text{Coulomb-friction:} \,\,\,  \tau_{\mathrm{s}}/N  = C_{\mathrm{c}}
318,319c317,318
< Here $\tau_{\mathrm{s}}$ is basal shear stress, $C_{\mathrm{s}}$ is
< a~sliding coefficient specific to each individual relation (Table
---
> Here $\tau_{\mathrm{s}}$ is basal shear stress; $C_{\mathrm{w}}$,
$C_{\mathrm{e}}$, and $C_{\mathrm{c}}$ are
> sliding coefficients specific to each individual relation (Table
321c320
< $\lambda_0$ is a~constant defining the overall bed geometry
---
> $\lambda_0$ is a~constant defining the overall bed geometry in the
Coulomb-friction sliding model
326c325
< sliding model and Columb-friction), which are both used in experiment
---
> sliding model and Coulomb-friction), which are both used in experiment
330c329
< influence of hydrology and assume that water pressure is everywhere
---
> influence of hydrology and initially assume that water pressure is everywhere
332c331
< $p_{\mathrm{w}}=0.8\rho_{\mathrm{i}}gH$. We note, however, that more complex
---
> $p_{\mathrm{w}}=0.8\rho_{\mathrm{i}}gH$. In the final experiment we
combine two additional flotation fractions of 70\% and 90\% with the
Coulomb-friction sliding relation to test the influence of water
pressure. We note, however, that more complex
338d336
<
343c341
<   \dot{e} = K_{\mathrm{a}}|\vec{u}_{\mathrm{s}}|^{m},
---
>   \dot{e} = K_{\mathrm{a}}u_{\mathrm{s}}^{m},
347,348c345,346
< $m$ is the erosion exponent and $\vec{u}_{\mathrm{s}}$ is sliding
< velocity. Parameters governing subglacial erosion through abrasion and
---
> $m$ is the erosion exponent and $u_{\mathrm{s}}$ is sliding
> rate. Parameters governing subglacial erosion through abrasion and
351c349
< quarrying \citep{Iverson12}. However, sliding-based erosions laws
---
> quarrying \citep{Iverson12}. However, sliding-based erosion laws
353c351
< \citep{harbor1992,seddik2005,pedersen2014}, which is why we use it
---
> \citep{harbor1992,seddik2005,pedersen2014}, which is why we use one
357,358c355,356
< phenomenological arguments than emperical evidence. We perform all
< erosional experiments with both a~linear ($m = 1$) and non-linear ($m
---
> phenomenological arguments (i.e. the erosion law leads to realistic
glacial landforms) than empirical evidence. We do however perform all
> erosion experiments with both a~linear ($m = 1$) and non-linear ($m
361c359
< \subsection{Comparing the output of iSOSIA and Elmer/ICE}
---
> \subsection{Comparing the output of iSOSIA and Elmer/Ice}
```

```
365c363
< Elmer/ICE, both models operate on the same synthetic input topography,
---
> Elmer/Ice, both models operate on the same synthetic input topography,
368,369c366,367
< grid, whereas for Elmer/ICE the two-dimensional grid is expanded to
< a~full three-dimensional mesh with five vertical levels. This gridding
---
> grid, whereas for Elmer/Ice the two-dimensional grid is extruded to
> a~full three-dimensional mesh with five vertical levels spanning the
thickness of the ice. This gridding
371c369
< input and mesh topology, except for Elmer/ICE having the additional
---
> input and mesh topology, except for Elmer/Ice having the additional
378,381c376
< Since Elmer/ICE computes stress and velocity on a~three-dimensional
< grid, post-processing is necessary in order to compare with iSOSIA.
< Horizontal stress and flow components from Elmer/ICE are therefore
< depth-averaged using the following function:
---
> Both models compute basal shear stress, $\vec{\tau}_{\mathrm{s}}$,
from the Cauchy stress tensor, $\sigma_{\mathrm{b}}$, at the bed:
383,391c378
<   \label{eq:depth-average}
<   \overline{u} =  \frac{1}{H} \int_0^H u(z) \mathrm{d}z,
< \end{align}
< where $u$ is the variable of interest (stress or velocity component),
< $z$ is depth below the ice surface and $H$ is local ice thickness.
<
< Both models compute basal shear stress as:
< \begin{align}
<   \vec{\tau}_{\mathrm{s}} = \sigma_{\mathrm{b}}\times \vec{n}_{\mathrm{b}} -
---
>   \vec{\tau}_{\mathrm{s}} = \sigma_{\mathrm{b}}\cdot \vec{n}_{\mathrm{b}} -
395,396c382
< where $\sigma_{\mathrm{b}}$ is the Cauchy stress tensor at the bed,
< and $\vec{\sigma}_{{n}}$ is the stress vector perpendicular to
---
> where  $\vec{\sigma}_{{n}}$ is the stress vector perpendicular to
399c385
<  \vec{\sigma}_{{n}} = (\vec{n}_{\mathrm{b}}\times  \sigma_{\mathrm{b}}\times
---
>  \vec{\sigma}_{{n}} = (\vec{n}_{\mathrm{b}}\cdot  \sigma_{\mathrm{b}}\cdot
403c389
< $\mathbf{n}_{\mathrm{b}}$ is the normal vector at the bed:
---
> and $\vec{n}_{\mathrm{b}}$ is the normal vector at the bed:
414a401,407
> We also compare the longitudinal and transverse stress components,
    $s_{xx}$, $s_{yy}$, and $s_{xy}$ from both models. However, since
    these are only computed by iSOSIA in a depth-averaged version, we
    need to depth-average the horizontal stress also from
    Elmer/Ice. We obtain the depth-averaging using the following function:
> \begin{align}
>   \label{eq:depth-average}
>   \overline{s}_{xx} =  \frac{1}{H} \int_0^H s_{xx}(z) \mathrm{d}z,
> \end{align}
> and similarly for $\overline{s}_{yy}$ and $\overline{s}_{xy}$. $z$
    is depth below the ice surface and $H$ is local ice thickness. We
    note that for Elmer/Ice the depth-averaged stress components do
    not enter the Cauchy stress tensor in Eq. \ref{eq:shearstress},
    which is instead constructed from the local stress state at the
    base of the ice.
```

```
>
416c409
< shear stress of iSOSIA and Elmer/ICE to the driving-stress
---
> shear stress of iSOSIA and Elmer/Ice to the driving-stress
430c423
< \subsection{Experiment 1 -- benchmarking steady-state solutions}
---
> \subsection{Experiment 1 -- comparing steady-state solutions}
434c427
< components from iSOSIA against those from Elmer/ICE. The steady-state
---
> components from iSOSIA against those from Elmer/Ice. The steady-state
441c434
< the main valley, reaching levels of 120\,\unit{m\,yr^{-1}}
---
> the main valley, reaching levels of 120\,\unit{m\,a^{-1}}
447c440
< by similar large-scale patterns in iSOSIA and Elmer/ICE
---
> by similar large-scale patterns in iSOSIA and Elmer/Ice
458,459c451
< flow direction.
<
---
> flow direction.\\
462c454
< $\overline{s}_{{xy}}$) in Elmer/ICE and iSOSIA are in general below
---
> $\overline{s}_{{xy}}$) in Elmer/Ice and iSOSIA are in general below
466d457
<
470c461
< 0.1\,\unit{MPa}. Differences between Elmer/ICE and iSOSIA are of order
---
> 0.1\,\unit{MPa}. Differences between Elmer/Ice and iSOSIA are of order
476,477c467,468
< 20\,\unit{m\,yr^{-1}} in the tributaries. Yet, the Elmer/ICE solution
< contains areas with high-frequency variations in basal sliding and
---
> 20\,\unit{m\,yr^{-1}} in the tributaries. Yet, the Elmer/Ice solution
> has areas with high-frequency variations in basal sliding and
479c470
< correlate with larger differences in sliding velocity between the two
---
> have larger differences in sliding velocity between the two
482c473
< To aid the comparison between iSOSIA and Elmer/ICE we extract stress
---
> To aid the comparison between iSOSIA and Elmer/Ice we extract stress
496,499c487,488
< stress, along the same profile, is 2 to 4 times greater in magnitude
< than the horizontal stress components, which reflects the influence of
< pressure, $p$, as well as the vertical shear stress components
< $s_{{xz}}$ and $s_{{yz}}$.
---
> stress along the profile is 2 to 4 times greater in magnitude
> than the horizontal stress components, which highlights how basal
    shear stress dominates the force balance of valley glaciers.
507c496
< remarkable constant along the profile and decreases only slightly
---
> remarkably constant along the profile and decreases only slightly
509,510c498,499
```

```
< significantly up-glacier. However, the effect of bed slope seems in
< this case to be counteracted by ice thinning.
---
> significantly up-glacier. However, in
> this case, the effect of bed slope is counteracted by ice thinning.
512c501
< There are no clear trends in misfit between iSOSIA and Elmer/ICE and
---
> There are no clear trends in misfit between iSOSIA and Elmer/Ice and
515c504
< high-frequency stress variations are slightly larger for Elmer/ICE
---
> high-frequency stress variations are slightly larger for Elmer/Ice
518,519c507,508
< SIA driving stress is generally higher, and show more intense
< variation, than the basal shear stress for both iSOSIA and Elmer/ICE.
---
> SIA driving stress is generally higher, and shows more intense
> variation, than the basal shear stress for both iSOSIA and Elmer/Ice.
526c515
< iSOSIA and Elmer/ICE results. Theoretically, increasing the relief
---
> iSOSIA and Elmer/Ice results. Theoretically, increasing the relief
532c521
< drainage patterns (Fig.~\ref{fig:exp2-topographies}c).  We then run
---
> drainage patterns (Fig.~\ref{fig:exp2-topographies}).  We then run
534c523
< topographies and transfer the resulting ice thicknesses to Elmer/Ice
---
> topographies and transfer the resulting ice thickness to Elmer/Ice
542c531
< components, which reflect local velocity gradients, also increase in
---
> components, which reflect local velocity gradients, also increases in
549,558c538,545
< In contrast to the englacial horizontal stress, the basal shear stress
< is remarkably unaffected by the increasing relief and remains rather
< uniform around 0.1--0.2\,\unit{MPa} for all four situations
< (Fig.~\ref{fig:exp2-all}).
<
<
< Examining differences between Elmer/ICE and iSOSIA, we note that both
< models agree on regional stress patterns and that iSOSIA stress
< follows the Elmer/ICE solution reasonably well across the range of
< reliefs tested here. The regional misfit remains small even when
---
> In contrast to the englacial horizontal stress, basal shear stress
> is almost unaffected by the increasing relief and the mean value
    remains around 0.2\,\unit{MPa} for all four situations
> (Fig.~\ref{fig:exp2-all}). The local deviation from this trend
    increases a bit from 0.02 to 0.05\,\unit{MPa} as the landscape steepens.
>
> Examining differences between Elmer/Ice and iSOSIA, we note that both
> models agree on regional stress patterns, and that iSOSIA stress
> follows the Elmer/Ice solution reasonably well across the range of
> relief tested here. The regional misfit remains small ($<$0.02 \,\unit{MPa}) even when
560,561c547
< however areas where the comparison exposes an increasing misfit
< between iSOSIA and Elmer/ICE, particularly when focussing on
---
> however areas where the comparison exposes an increasing misfit (up
    to 0.1 \,\unit{MPa}) between iSOSIA and Elmer/Ice, particularly when focussing on
566c552
```

```
< Unlike the basal shear stress from iSOSIA and Elmer/ICE, both regional
---
> Unlike the basal shear stress from iSOSIA and Elmer/Ice, both regional
569c555
< Elmer/ICE and iSOSIA are in the order of 0--0.05\,\unit{MPa} for
---
> Elmer/Ice and iSOSIA are on the order of 0--0.05\,\unit{MPa} for
571c557
< misfit between SIA and Elmer/ICE quickly reaches levels well above
---
> misfit between SIA and Elmer/Ice quickly reaches levels well above
578c564
< After evaluating steady-state solutions of iSOSIA against Elmer/ICE we
---
> After evaluating steady-state solutions of iSOSIA against Elmer/Ice we
581,584c567,570
< only use iSOSIA for this experiment as the computational costs of
< Elmer/ICE prevents us from running simulations over the thousand year
< timescales required for glacial landscape development. The initial
< topography from experiment 1 is used as input for iSOSIA and is slowly
---
> only used iSOSIA for this experiment as the computational costs of
> Elmer/Ice prevent us from running simulations over the thousand year
> time-scales required for glacial landscape development. The initial
> topography from experiment 1 was used as input for iSOSIA and was slowly
587c573
< First, we run the experiment using the Weertman relation for sliding
---
> First, we ran the experiment using the Weertman relation for sliding
596c582
< valley floors, hanging valleys and truncated spurs.
---
> valley floors, hanging valleys and truncated spurs (Fig. ~\ref{fig:exp3-3d-landscape}b)
603c589
< that obstruct flow. This development generally cause bed shear stress
---
> that obstruct flow. This development generally causes bed shear stress
605c591
< the ice (Fig.~\ref{fig:exp3-landscape-evolution}). This reduction in
---
> the ice (Fig.~\ref{fig:exp3-landscape-evolution}). The reduction in
610c596
< To test the robustness of this trend we repeat experiment 3 using two
---
> To test the robustness of this trend we repeated experiment 3 using two
614,615c600,601
< \citep[Eq.~\ref{eq:cf};][]{schoof_effect_2005,Gagliardini2007} as well
< as a~linear erosion law ($m=1$ in Eq.~\ref{eq:erosion}).  The three
---
> \citep[Eq.~\ref{eq:cf};][]{schoof_effect_2005,Gagliardini2007}. The
    different sliding coefficients (Table \ref{tab:settings}) were calibrated to give sim
> The three
619,620c605,606
< initially lead to high values of shear stress in the trunk valley and
< upper tributaries, and short-scale variations that mimic the details
---
> predict high shear stress in the trunk valley and
> upper tributaries, and short-scale stress variations that mimic the details
623,624c609
< stress. This effect is strongest for the Weertman and Columb-friction
< relations.  As a~consequence of the decreasing stress, the spatially
---
> stress. This effect is strongest for the Weertman relation but occur
    for all three relations. As a~consequence of the decreasing stress, the spatially
```

```
626,628c611,616
< erosion in the trunk valley, which is largely independent of the
< exponent, $m$, in the erosion rule
< (Fig.~\ref{fig:exp3-erosionandsliding}). The latter underlines that
---
> erosion in the trunk valley (Fig.~\ref{fig:exp3-erosionandsliding}a).
>
> To further test the robustness of this trend, we repeated the
    experiments using: 1) a~linear erosion law ($m=1$ in
    Eq.~\ref{eq:erosion}) in combination with all three sliding laws
    (Fig.~\ref{fig:exp3-erosionandsliding}b), and 2) the
    Coulomb-friction sliding model using two alternative flotation
    fractions ($70\%$ and $90\%$) to compute effective pressure, $N$ (Fig.~\ref{fig:exp3-
> The similar outcome of these final experiments suggests that
    decreasing basal shear stress in response to erosion is largely independent of hydrol
> exponent, $m$, in the erosion equation
> (Fig.~\ref{fig:exp3-erosionandsliding}). The latter indicates that
639c627
< different computational methods: iSOSIA and Elmer/ICE. The comparison
---
> different computational methods: iSOSIA and Elmer/Ice. The comparison
646,647c634,635
< the objective of the benchmarking experiments is to estimate the
< {difference} between stress predicted by the two methods under
---
> the objective of the comparison study is to estimate the
> difference between stress predicted by the two methods under
650c638
< topography and ice distribution, as well as the same horizontal grid
---
> topography and ice distribution, as well as the same horizontal Cartesian grid
652c640
< Elmer/ICE). We note here that the true accuracy of both methods is
---
> Elmer/Ice). We note here that the true accuracy of both methods is
654c642
< method in Elmer/ICE allows irregular grid structures that may increase
---
> method in Elmer/Ice allows irregular grid structures that may increase
659c647
< equations is not meaningful if similar meshes are not used.
---
> equations is only meaningful if similar meshes are used.
661c649
< The benchmark experiments show that iSOSIA and Elmer/ICE predict the
---
> The comparison study shows that iSOSIA and Elmer/Ice predict the
669,671c657,659
< difference in results from iSOSIA and Elmer/ICE seems to be confined
< to spatial scales of few hundred meters (i.e. the grid cell
< spacing). In particular, Elmer/ICE includes high-frequency
---
> difference in results from iSOSIA and Elmer/Ice seems to be confined
> to spatial scales of few hundred meters (i.e. the grid-cell
> spacing). In particular, Elmer/Ice includes high-frequency
677,681c665,668
< in sliding velocity between neighbouring grid cells in Elmer/ICE are
< surprising and cannot easily be explained by variations in bed
< topography.
<
< The high-frequency variations of Elmer/ICE are amplified slightly when
---
> in sliding velocity between neighbouring grid cells in Elmer/Ice are
> surprising and cannot readily be explained by variations in bed
```

```
> topography. We therefore ascribe these high-frequency stress
    variations in Elmer/Ice to the ice thickness configuration used,
    which was generated using iSOSIA and therefore in balance with the
    governing equations of this ice model. Elmer/Ice is not allowed to
    make adjustments to the ice thickness, that would otherwise dampen the local stress v
> The high-frequency variations of Elmer/Ice are amplified slightly when
684c671
< accordance between iSOSIA and Elmer/ICE stress predictions seems
---
> accordance between iSOSIA and Elmer/Ice stress predictions seems
693,695c680,682
< transformation from a~fluvial to a~glacial topography. We observe this
< trend for all sliding laws tested in this study (Weertmann, empirical,
< Columb-friction; Fig.~\ref{fig:exp3-tsPanel}) and for two different
---
> transformation from a~fluvial to a~glacial topography. This
> trend can be recognized for all sliding laws tested in this study (Weertmann, empirical
> Coulomb-friction; Fig.~\ref{fig:exp3-tsPanel}) and for two different
698,699c685,686
< The highest initial levels of basal shear stress are associated with
< bends in the fluvial channel profile that forms interlocking spurs
---
> The highest basal shear stress is associated with
> bends in the fluvial channel profile that form interlocking spurs
701,702c688,689
< by glacial erosion which decreases basal shear stress.  In the main
< valley, glacial erosion thereby efficiently remove obstacles and
---
> by glacial erosion and this decreases basal shear stress.  In the main
> valley, glacial erosion thereby efficiently removes obstacles and
711c698
< through the sliding relations (Eqs. \ref{eq:weertman}--\ref{eq:cf}),
---
> through a sliding relation (Eqs. \ref{eq:weertman}--\ref{eq:cf}),
718,719c705,706
< in topographic features that resembles well-known glacial landforms,
< and it seems reasonably that smoother and flatter post-glacial
---
> in topographic features that resemble well-known glacial landforms,
> and it seems reasonable that smoother and flatter post-glacial
722d708
<
726c712
< relations used. Two of the sliding relations have a~power-law scaling
---
> relations used. All of the sliding relations have a~power-law scaling
728,735c714,717
< shear stress (the Weertman and the empirical sliding relations). The
< Coulomb-friction sliding model, on the other hand, operates with an
< upper limit to the bed's ability to support shear stress (the bed
< resistance). In addition to the sliding rate, the upper stress limit
< (the bed resistance) associated with Coulomb-friction depends on water
< pressure and the bed roughness, which is controlled by parameters
< $C_{\mathrm{s}}$ and $\lambda_0$ in Eq.~(\ref{eq:cf}). Here we
< speculate, that if the bed resistance decreases more rapidly than the
---
> shear stress (the power-law scaling of the Coulomb-friction sliding model occurs below
> upper limit to the bed's ability to support shear stress). In
    addition to the sliding rate, basal shear stress associated with
    the sliding models depends on bed resistance and roughness, which is controlled by pa
> $C_{\mathrm{w}}$, $C_{\mathrm{e}}$, $C_{\mathrm{c}}$ and $\lambda_0$ in Eqs.~(\ref{eq:w
> speculate, that if bed resistance decreases more rapidly than the
737c719
< possibly accelerate as the topography is eroded in contrast to the
```

```
---
> possibly accelerate as topography is eroded, in contrast to the
739c721
< example, the bed is smoothened by erosion or if the flatter glacial
---
> example, the bed is smoothed by erosion or if the flatter glacial
742,744c724,725
< because we ignore effects of melt-water hydrology, and partly because
< the parameters representing bed roughness ($C_{\mathrm{s}}$ and
< $\lambda_0$ in Eq.~\ref{eq:cf}) are treated as constants independent
---
> because we ignore complex effects of melt-water hydrology, and partly because
> the sliding parameters representing bed roughness are treated as constants independent
753,754c734,735
< in the initial phase of glacial landscape evolution, when landforms
< are unadapted to the new glacial regime \citep{harbor1992,Braun99}. In
---
> in the initial phase of glacial landscape evolution, before landforms
> are adapted to the new glacial regime \citep{harbor1992,Braun99}. In
756c737
< processes not accounted here, such as a~transient climate forcing
---
> processes not accounted for here, such as a~transient climate forcing
762c743
< fracturing in response to high differential in situ stresses
---
> fracturing in response to high differential stresses
769c750
< (iSOSIA) and a~full-Stokes three-dimensional model (Elmer/ICE). Using
---
> (iSOSIA) and a~full-Stokes model (Elmer/Ice). Using
775c756
< \item iSOSIA and Elmer/ICE produce stress and sliding patterns that
---
> \item iSOSIA and Elmer/Ice produce stress and sliding patterns that
778c759
<   insensitive to increases in overall relief, as reduction on ice
---
>   insensitive to increases in overall relief, as reduction in ice
796,797c777,778
<   Elmer/ICE. C.~F.~Br{\ae}dstrup prepared the manuscript with
<   contributions from all co-authors.}
---
>   Elmer/Ice. C.~F.~Br{\ae}dstrup and D.~L.~Egholm prepared the manuscript with
>   contributions from co-authors.}
800,801c781,782
<   We thank Thomas Zwinger from the Elmer/ICE team for invaluable help
<   with initial model setup.  This research was funded by The Danish
---
>   We thank Thomas Zwinger from the Elmer/Ice team for invaluable help
>   with model set-up.  Associate editor Michelle Koppes and two
    anonymous reviewers are thanked for constructive comments and
    suggestions that improved the manuscript. The study was funded by The Danish
806a788,792
> \bibitem[{Adhikari et~al.(2013),Adhikari and Marshall}]{adhikari2013}
> Adhikari,~S., and Marshall,~S.~J.: Influence of high-order mechanics
> on simulation of glacier response to climate change: insights from
> Haig Glacier, Canadian Rocky Mountains, The Cryosphere, 7,
    1527--1541, doi:\href{http://dx.doi.org/10.5194/tc-7-1527-2013}{10.5194/tc-7-1527-201
>
1065c1051
< \bibitem[{Stokes(1845)}]{stokes1845}
---
> \bibitem[{Stokes(1845)}]{Stokes1845}
```

```
1101c1087
< $A$  & Ice flow parameter & $1 \times 10^{-16}$\,\unit{Pa^{-3}\,yr^{-1}}\\
---
> $A$  & Ice flow parameter & $1 \times 10^{-16}$\,\unit{Pa^{-3}\,a^{-1}}\\
1103,1108c1089,1094
< $C_{\mathrm{s}}$  & Weertman sliding coefficient & $2\times 10^{-9}$\,\unit{m\,Pa^{-2}\
< $C_{\mathrm{s}}$  & Empirical sliding coefficient  & $2 \times 10^{-3}$\,\unit{m\,Pa^{-
< $C_{\mathrm{s}}$  & Columb-friction sliding coefficient  & {0.25}\\
< $\lambda_0$  & Columb-friction sliding parameter  & $2 \times 10^{-17}$\,\unit{m\,Pa^{-
< $m_{\text{acc}}$  & Accumulation gradient & 0.5\,\unit{m\,yr^{-1}\,{\degree}C^{-1}} \\
< $m_{\text{alb}}$  & Ablation gradient & 1.5\,\unit{m\,yr^{-1}\,{\degree}C^{-1}} \\
---
> $C_{\mathrm{w}}$  & Weertman sliding coefficient & $2\times 10^{-9}$\,\unit{m\,Pa^{-2}\
> $C_{\mathrm{e}}$  & Empirical sliding coefficient  & $5 \times 10^{-9}$\,\unit{m\,Pa^{-
> $C_{\mathrm{c}}$  & Coulomb-friction sliding coefficient  & {0.25}\\
> $\lambda_0$  & Coulomb-friction sliding parameter  & $2 \times 10^{-17}$\,\unit{m\,Pa^{
> $m_{\text{acc}}$  & Accumulation gradient & 0.5\,\unit{m\,a^{-1}\,{\degree}C^{-1}} \\
> $m_{\text{alb}}$  & Ablation gradient & 1.5\,\unit{m\,a^{-1}\,{\degree}C^{-1}} \\
1110c1096,1098
< $K_{\mathrm{a}}$  & Subglacial abrasion erosion constant & $2.5\times 10^{-6}$\,\unit{m
---
> $K_{\mathrm{a}}$  & Subglacial abrasion erosion constant & \\
> & \hspace{0.5cm} for $m=1$ & $8\times 10^{-5}$\\
> & \hspace{0.5cm} for $m=2$ & $2.5\times 10^{-6}$\,\unit{m^{-1}\,a}\\
1118d1105
<
1120c1107
<   \includegraphics[width=120mm]{esurf-2015-17-discussions-f01.png}
---
>   \includegraphics[width=120mm]{esurf-2015-17-revised-f01.png}
1131c1118
<   \includegraphics[height=110mm]{esurf-2015-17-discussions-f02.png}
---
>   \includegraphics[height=110mm]{esurf-2015-17-revised-f02.png}
1133c1120
<     Elmer/ICE shown in top view. The first two columns show the
---
>     Elmer/Ice shown in top view. The first two columns show the
1136c1123
<     column shows the difference between iSOSIA and Elmer/ICE
---
>     column shows the difference between iSOSIA and Elmer/Ice
1146,1147c1133,1134
<   \includegraphics[width=120mm]{esurf-2015-17-discussions-f03.png}
<   \caption{iSOSIA (orange) and Elmer/ICE (green) stress components
---
>   \includegraphics[width=120mm]{esurf-2015-17-revised-f03.png}
>   \caption{iSOSIA (orange) and Elmer/Ice (green) stress components in \unit{MPa}
1149c1136
<     profile in \unit{MPa}. Upper three rows compare the higher-order
---
>     profile. Upper three rows compare the higher-order depth-averaged
1157c1144,1145
<     shown in the bottom right panel.}
---
>     shown in the bottom right panel. Note that the bottom row are map views of the
>   3D model (Fig. ~\ref{fig:exp1-3d}a, b).}
1164c1152
<   \includegraphics[height=110mm]{esurf-2015-17-discussions-f04.png}
---
>   \includegraphics[height=110mm]{esurf-2015-17-revised-f04.png}
1176c1164
<   \includegraphics[width=120mm]{esurf-2015-17-discussions-f05.png}
---
```

```
>   \includegraphics[width=120mm]{esurf-2015-17-revised-f05.png}
1178c1166
<     Elmer/ICE (green) for the increasing topographical relief in
---
>     Elmer/Ice (green) for the increasing topographical relief in
1183c1171
<     comparison (blue line). Forth row shows the ice-surface and bed
---
>     comparison (blue line). Fourth row shows the ice-surface and bed
1192,1200c1180,1190
<   \includegraphics[width=120mm]{esurf-2015-17-discussions-f06.png}
<   \caption{Preglacial landscape showing the initial fluvial topography
<     \textbf{(a)}. The postglacial landscape after 100\,\unit{m} of
<     average erosion (using $m=2$ in
<     Eq.~\ref{eq:erosion}). \textbf{(b)}. Several characteristic
<     features of glaciated landscapes are evident in \textbf{(b)}. The
<     trunk valley is widened with steep slopes along the sides forming
<     a~U-shaped cross section. Flattened valley floors, hanging valleys
<     and truncated spurs are also visible.}
---
>   \includegraphics[width=120mm]{esurf-2015-17-revised-f06.pdf}
>   \caption{textbf{(a)} Preglacial landscape with initial fluvial
    topography. \textbf{(b)} The landscape after 100\,\unit{m} average glacial erosion (u
>     Eq.~\ref{eq:erosion}) . Several characteristic
>     glacial landforms are evident in
>     the eroded landscape. Highlighted with numbered arrows are:
>     (1) flattened valley floor, (2) a hanging valley, and (3) a
>     truncated spur. The
>     main valley is widened forming
>     a~U-shaped cross-section with steep slopes along the sides. \textbf{(c)} The total
>     erosion. Erosion is concentrated in the
>     main trunk valley along the truncated spurs and at high elevation near the headwall
1207c1197
<   \includegraphics[width=120mm]{esurf-2015-17-discussions-f07.pdf}
---
>   \includegraphics[width=120mm]{esurf-2015-17-revised-f07.pdf}
1219c1209
<   \includegraphics[width=120mm]{esurf-2015-17-discussions-f08.pdf}
---
>   \includegraphics[width=120mm]{esurf-2015-17-revised-f08.pdf}
1224c1214
<     Columb-friction (Eq.~\ref{eq:cf}) at different stages of glacial
---
>     Coulomb-friction (Eq.~\ref{eq:cf}) at different stages of glacial
1232,1236c1222,1226
<   \includegraphics[width=120mm]{esurf-2015-17-discussions-f09.pdf}
<   \caption{Evolution of normalised mean sliding rate as a~function of
<     mean erosion for three different sliding laws. \textbf{(a)} Shows
<     results using a~linear erosion law ($m=1$ in
<     Eq.~\ref{eq:erosion}). \textbf{(b)} Results using $m=2$. The means
---
>   \includegraphics[width=120mm]{esurf-2015-17-revised-f09.pdf}
>   \caption{Evolution of mean sliding rate as a~function of
>     mean erosion. \textbf{(a)} Shows
>     results for three different sliding laws using a~non-linear erosion law ($m=2$ in
>     Eq.~\ref{eq:erosion}) and 80$\%$ floatation. \textbf{(b)} The
    same as \textbf{(a)} but for $m=1$. \textbf{(c)} The evolution of
    mean sliding for the Coulomb-friction sliding law and three different levels of float
1245a1236,1240
>
> %%% Local Variables:
> %%% mode: latex
> %%% TeX-master: t
> %%% End:
```